

Efficient verification of Affleck-Kennedy-Lieb-Tasaki states

Tianyi Chen,^{1,2,3,*} Yunting Li,^{1,2,3,*} and Huangjun Zhu^{1,2,3,†}

¹*State Key Laboratory of Surface Physics and Department of Physics, Fudan University, Shanghai 200433, China*

²*Institute for Nanoelectronic Devices and Quantum Computing, Fudan University, Shanghai 200433, China*

³*Center for Field Theory and Particle Physics, Fudan University, Shanghai 200433, China*

(Dated: July 1, 2022)

Affleck-Kennedy-Lieb-Tasaki (AKLT) states are an important class of many-body quantum states that are useful in quantum information processing, including measurement-based quantum computation in particular. Here we propose a general approach for constructing efficient verification protocols for AKLT states on arbitrary graphs with local spin measurements. Our verification protocols build on bond verification protocols and matching covers (including edge coloring) of the underlying graphs, which have a simple geometric and graphic picture. We also provide rigorous performance guarantee that is required for practical applications. With our approach, most AKLT states of wide interest, including those defined on 1D and 2D lattices, can be verified with a constant sample cost, which is independent of the system size and is dramatically more efficient than all previous approaches. As an illustration, we construct concrete verification protocols for AKLT states on various lattices and on arbitrary graphs up to five vertices.

I. INTRODUCTION

Ground states of local Hamiltonians play crucial roles in many-body physics and have also found increasing applications in quantum information processing [1–6]. The Affleck-Kennedy-Lieb-Tasaki (AKLT) states [7, 8] are of special interest because they are the ground states of exactly solvable models and are tied to the famous Haldane conjecture [9, 10]. These states are originally defined on spin chains and have been generalized to arbitrary graphs later [11–13]. Recently, AKLT states have attracted increasing attention because of their connection with symmetry-protected topological orders [14–16]. Moreover, AKLT states on many 2D lattices, including the honeycomb lattice, are universal resource states for measurement-based quantum computation [17–21].

In practice it is not easy to prepare many-body states, such as AKLT states, perfectly. Therefore, it is crucial to verify these states within a desired precision efficiently. However, traditional tomographic approaches are too resource consuming to achieve this goal for large and intermediate quantum systems. Recently, great efforts have been directed to addressing this problem [22–26], and various alternative approaches have been proposed, including compressed sensing [27], direct fidelity estimation [28, 29], and shadow estimation [30, 31] etc.

Here we are particularly interested in a promising approach known as quantum state verification (QSV), which can achieve high efficiency based on local measurements [32–42]. So far efficient verification protocols have been constructed for bipartite pure states [32, 36, 43–47], stabilizer states (including graph states and Greenberger-Horne-Zeilinger states in particular) [36, 39, 48–53], hypergraph states [52], weighted graph states [54], Dicke

states [55], and phased Dicke states (including Slater determinant states) [55, 56]. In addition, several verification protocols have been demonstrated successfully in experiments [57–60]. Moreover, this approach can be generalized to the verification of quantum gates and processes [61–64], which have also been demonstrated in experiments [65, 66]. Unfortunately, efficient verification protocols known so far are usually tailored to quantum states with special structures and rely on explicit expressions of the states under consideration. For the ground states of local Hamiltonians, although several verification protocols have been proposed [33, 35, 37, 67, 68], it is still too resource consuming to verify large and intermediate quantum systems.

In this paper, following the simple recipe proposed in the companion paper [69], we propose a general approach for constructing efficient verification protocols for AKLT states defined on arbitrary graphs. Notably, explicit expressions for the AKLT states are not necessary. Our verification protocols are based on local spin measurements and are thus easy to implement in experiments. In addition, these verification protocols have very simple description in terms of elementary geometric and graph theoretic concepts. Moreover, we provide rigorous upper bounds on the number of tests (sample cost) required to achieve a given precision. With our approach, most AKLT states of practical interest, including those defined on 1D and 2D lattices, can be verified with a number of tests that is independent of the system size, which is dramatically more efficient than previous approaches [33, 35, 37, 68]. In addition, we construct concrete verification protocols for all AKLT states defined on arbitrary graphs up to five vertices.

The rest of this paper is organized as follows. In Sec. II we first review the basic framework of QSV and then introduce the idea of subspace verification as a generalization. In Sec. III we review the definition and basic properties of AKLT states that are relevant in later studies. In Sec. IV we clarify potential bond test operators

* These authors contributed equally to this work.

† zhu Huangjun@fudan.edu.cn

based on spin measurements and construct various optimal and efficient bond verification protocols. In Sec. V we propose a general approach for constructing efficient verification protocols for AKLT states together with rigorous performance guarantee. In Sec. VI we discuss in detail the verification of 1D AKLT states. In Sec. VII we construct concrete verification protocols for AKLT states defined on general graphs up to five vertices. In Sec. VIII we summarize this paper. Several technical proofs and a table are relegated to the Appendix.

II. QUANTUM STATE VERIFICATION

In this section we first review the general framework of QSV following Refs. [36, 38, 39]. Then we generalize the idea to subspace verification, which is closely tied to the verification of ground states of local Hamiltonians.

A. Basic framework

A primitive in quantum information processing is to produce a given quantum state $|\Psi\rangle$ with prescribed properties. In practice, the device we employ is never perfect, and the states produced in individual runs may be different from the target state and also different from each other. So it is crucial to verify whether the deviation from the target state, usually quantified by the infidelity, is tolerable. To address this problem, in each run we can perform a random two-outcome measurement $\{T_l, 1-T_l\}$ determined by the test operator T_l , where the two outcomes correspond to passing and failing the test, respectively. To guarantee that the target state $|\Psi\rangle$ can pass the test with certainty, the test operator T_l needs to satisfy the following requirement

$$T_l|\Psi\rangle = |\Psi\rangle. \quad (1)$$

Let p_l be the probability of performing the test T_l and define the *verification operator*

$$\Omega = \sum_l p_l T_l. \quad (2)$$

Suppose σ is a quantum state whose fidelity with the target state is at most $1 - \epsilon$, that is, $\langle\Psi|\sigma|\Psi\rangle \leq 1 - \epsilon$; then the probability that σ can pass each test on average is bounded from above as follows [36, 38, 39],

$$\max_{\langle\Psi|\sigma|\Psi\rangle \leq 1-\epsilon} \text{tr}(\Omega\sigma) = 1 - [1 - \beta(\Omega)]\epsilon = 1 - \nu(\Omega)\epsilon, \quad (3)$$

where $\beta(\Omega)$ denotes the second largest eigenvalue of the verification operator Ω , and $\nu(\Omega) = 1 - \beta(\Omega)$ is referred to as the *spectral gap*.

As a corollary of Eq. (3) the probability that the states $\sigma_1, \sigma_2, \dots, \sigma_N$ can pass all N tests satisfies [36, 38, 39]

$$\prod_{j=1}^N \text{tr}(\Omega\sigma_j) \leq \prod_{j=1}^N [1 - \nu(\Omega)\epsilon_j] \leq [1 - \nu(\Omega)\bar{\epsilon}]^N, \quad (4)$$

where $\epsilon_j = 1 - \langle\Psi|\sigma_j|\Psi\rangle$ is the infidelity of the state σ_j and $\bar{\epsilon} = \sum_j \epsilon_j/N$ is the average infidelity. To verify the target state $|\Psi\rangle$ within infidelity ϵ and significance level δ , which means $\delta \geq [1 - \nu(\Omega)\epsilon]^N$, the minimum number of tests required is given by [36, 38, 39]

$$N = \left\lceil \frac{\ln \delta}{\ln[1 - \nu(\Omega)\epsilon]} \right\rceil \approx \frac{\ln(\delta^{-1})}{\nu(\Omega)\epsilon}, \quad (5)$$

which decreases monotonically with the spectral gap $\nu(\Omega)$. To achieve a high efficiency, we need to construct a verification operator with a large spectral gap. Here we shall focus on verification protocols that can be realized by local projective measurements, which are most amenable to practical applications.

The verification operator Ω is *homogeneous* [38, 39, 44] if it has the form

$$\Omega = |\Psi\rangle\langle\Psi| + \lambda(1 - |\Psi\rangle\langle\Psi|). \quad (6)$$

In this case, the probability that σ can pass each test on average is completely determined by its fidelity with the target state $|\Psi\rangle$,

$$\text{tr}(\Omega\sigma) = \lambda + \nu F = 1 - \nu\epsilon, \quad (7)$$

where $F = \langle\Psi|\sigma|\Psi\rangle$ and $\epsilon = 1 - F$. Such verification protocols are of special interest because they can also be used for fidelity estimation.

B. Subspace verification

The basic idea of QSV can also be applied to subspace verification, which emerges naturally in the verification of multipartite pure states, such as the ground states local Hamiltonians. To see this point, suppose we want to verify the multipartite pure state $|\Psi\rangle$ whose reduced states are mixed and are supported in certain subspaces. To this end, we can verify that each reduced state is supported in a particular subspace. Quite often it turns out that the target state $|\Psi\rangle$ can be verified in this way without additional steps. Notably, this strategy is particularly useful to verifying the ground states of frustrate-free Hamiltonians, including AKLT states in particular.

Let \mathcal{V} be a given subspace of the Hilbert space \mathcal{H} under consideration and Q the corresponding projector. Our task is to verify whether the state produced is supported in this subspace. To address this problem, we can construct a set of tests and perform a random test from this set in each run. Every test corresponds to a two-outcome measurement $\{T_l, 1-T_l\}$, which is determined by the test operator T_l , as in the verification of a pure state. Now the condition in Eq. (1) is replaced by

$$T_l Q = Q, \quad (8)$$

so that all states supported in \mathcal{V} can pass each test with certainty. Let p_l be the probability of performing the test

T_l and define the verification operator

$$\Omega = \sum_l p_l T_l \quad (9)$$

as in QSV [cf. Eq. (2)]. Then Ω satisfies the condition $\Omega Q = Q$ thanks to Eq. (8).

Suppose the quantum state σ under consideration satisfies the condition $\text{tr}(Q\sigma) \leq 1 - \epsilon$; then the probability that σ can pass each test on average is bounded from above as follows,

$$\max_{\text{tr}(Q\sigma) \leq 1 - \epsilon} \text{tr}(\Omega\sigma) = 1 - [1 - \beta(\Omega)]\epsilon = 1 - \nu(\Omega)\epsilon, \quad (10)$$

where

$$\beta(\Omega) = \|\bar{\Omega}\|, \quad \nu(\Omega) = 1 - \beta(\Omega), \quad (11)$$

$$\bar{\Omega} = (1 - Q)\Omega(1 - Q). \quad (12)$$

As a corollary of Eq. (10), the probability that the states $\sigma_1, \sigma_2, \dots, \sigma_N$ produced in N runs can pass all N tests satisfies

$$\prod_{j=1}^N \text{tr}(\Omega\sigma_j) \leq \prod_{j=1}^N [1 - \nu(\Omega)\epsilon_j] \leq [1 - \nu(\Omega)\bar{\epsilon}]^N, \quad (13)$$

where $\epsilon_j = 1 - \text{tr}(Q\sigma_j)$ and $\bar{\epsilon} = (\sum_j \epsilon_j)/N$. This result has the same form as the counterpart in QSV. To verify the subspace \mathcal{V} within infidelity ϵ and significance level δ , the number of tests required reads

$$N = \left\lceil \frac{\ln \delta}{\ln[1 - \nu(\Omega)\bar{\epsilon}]} \right\rceil \approx \frac{\ln(\delta^{-1})}{\nu(\Omega)\bar{\epsilon}}, \quad (14)$$

which also has the same form as the counterpart in QSV as presented in Eq. (5).

The concept of homogeneous verification operators has a natural generalization in the context of subspace verification. Now the verification operator Ω is *homogeneous* if it has the form

$$\Omega = Q + \lambda(1 - Q). \quad (15)$$

In this case, the probability that σ can pass each test on average is completely determined by the overlap $\text{tr}(Q\sigma)$,

$$\text{tr}(\Omega\sigma) = \lambda + \nu \text{tr}(Q\sigma) = 1 - \nu[1 - \text{tr}(Q\sigma)]. \quad (16)$$

In other words, the overlap $\text{tr}(Q\sigma)$ can be estimated from the passing probability $\text{tr}(\Omega\sigma)$. Such verification protocols will play an important role in the verification of AKLT states, as we shall see shortly.

III. AKLT STATES

In this section we briefly review AKLT states defined on general graphs [7, 8, 11–13]. For the convenience of the readers, basic facts about spin operators and graphs are introduced in advance.

A. Spin operators

The spin operator associated with a spin- S particle is denoted by $\mathbf{S} = (S_x, S_y, S_z)$, where S_x, S_y, S_z are the spin operators along directions $\hat{x}, \hat{y}, \hat{z}$, respectively, which act on a Hilbert space of dimension $2S + 1$. Note that S_x, S_y, S_z are nondegenerate and have eigenvalues $S, S - 1, \dots, -S$. Given an eigenvalue m of S_z , the corresponding eigenstate is denoted by $|S, m\rangle$ or $|m\rangle$ when S is clear from the context. Then the operators S_x, S_y, S_z can be expressed as

$$S_x = \frac{S_+ + S_-}{2}, \quad S_y = \frac{S_+ - S_-}{2i}, \quad S_z = \sum_{m=-S}^S m |m\rangle\langle m|, \quad (17)$$

where

$$S_+ = \sum_{m=-S}^{S-1} \sqrt{S(S+1) - m(m+1)} |m+1\rangle\langle m|, \quad (18)$$

$$S_- = \sum_{m=-S+1}^S \sqrt{S(S+1) - m(m-1)} |m-1\rangle\langle m|.$$

When $S = 1$ for example, S_x, S_y, S_z have the following matrix representations,

$$S_x = \frac{1}{\sqrt{2}} \begin{pmatrix} 0 & 1 & 0 \\ 1 & 0 & 1 \\ 0 & 1 & 0 \end{pmatrix}, \quad S_y = \frac{i}{\sqrt{2}} \begin{pmatrix} 0 & -1 & 0 \\ 1 & 0 & -1 \\ 0 & 1 & 0 \end{pmatrix}, \quad (19)$$

$$S_z = \begin{pmatrix} 1 & 0 & 0 \\ 0 & 0 & 0 \\ 0 & 0 & -1 \end{pmatrix}.$$

Let \mathbf{r} be a (real) unit vector in dimension 3, then the spin operator along direction \mathbf{r} reads

$$S_{\mathbf{r}} := \mathbf{r} \cdot \mathbf{S} = r_x S_x + r_y S_y + r_z S_z. \quad (20)$$

Note that $S_{\mathbf{r}}$ has the same eigenvalues as S_z for any unit vector \mathbf{r} in dimension 3. The eigenstate of $S_{\mathbf{r}}$ associated with the eigenvalue m is denoted by $|S, m\rangle_{\mathbf{r}}$ or $|m\rangle_{\mathbf{r}}$ when S is clear from the context. When $m = S$ ($m = -S$), the eigenstate is also denoted by $|+\rangle_{\mathbf{r}}$ ($|-\rangle_{\mathbf{r}}$). The projector onto $|m\rangle_{\mathbf{r}}$ can be expressed as

$$|m\rangle_{\mathbf{r}}\langle m| = \prod_{k=-S, k \neq m}^S \frac{S_{\mathbf{r}} - k}{m - k}, \quad (21)$$

which implies that

$$|+\rangle_{\mathbf{r}}\langle +| = |S\rangle_{\mathbf{r}}\langle S| = \prod_{k=-S}^{S-1} \frac{S_{\mathbf{r}} - k}{S - k}, \quad (22)$$

$$|-\rangle_{\mathbf{r}}\langle -| = |-S\rangle_{\mathbf{r}}\langle -S| = \prod_{k=-S+1}^S \frac{S_{\mathbf{r}} - k}{-S - k}.$$

In the special case $S = 1/2$, Eq. (22) yields

$$|\pm\rangle_{\mathbf{r}}\langle\pm| = \left|\pm\frac{1}{2}\right\rangle_{\mathbf{r}}\left\langle\pm\frac{1}{2}\right| = \frac{1}{2} \pm S_{\mathbf{r}} = \frac{1 \pm \mathbf{r} \cdot \boldsymbol{\sigma}}{2}, \quad (23)$$

where $\boldsymbol{\sigma} = (\sigma_x, \sigma_y, \sigma_z)$ is the vector composed of the three Pauli operators. When $S = 1$ by contrast, Eq. (21) yields

$$|\pm\rangle_{\mathbf{r}}\langle\pm| = \frac{S_{\mathbf{r}}(S_{\mathbf{r}} \pm 1)}{2}, \quad |0\rangle_{\mathbf{r}}\langle 0| = 1 - S_{\mathbf{r}}^2. \quad (24)$$

In addition, given two unit vectors \mathbf{r}, \mathbf{s} in dimension 3, the fidelities between $|\pm\rangle_{\mathbf{r}}$ and $|\pm\rangle_{\mathbf{s}}$ read (cf. Sec. III D in Ref. [70])

$$\begin{aligned} |\mathbf{r}\langle + | + \rangle_{\mathbf{s}}|^2 &= |\mathbf{r}\langle - | - \rangle_{\mathbf{s}}|^2 = \left(\frac{1 + \mathbf{r} \cdot \mathbf{s}}{2}\right)^{2S}, \\ |\mathbf{r}\langle + | - \rangle_{\mathbf{s}}|^2 &= |\mathbf{r}\langle - | + \rangle_{\mathbf{s}}|^2 = \left(\frac{1 - \mathbf{r} \cdot \mathbf{s}}{2}\right)^{2S}. \end{aligned} \quad (25)$$

When $S = 1/2$, Eq. (25) yields the familiar fidelity formula for a qubit,

$$\begin{aligned} |\mathbf{r}\langle + | + \rangle_{\mathbf{s}}|^2 &= |\mathbf{r}\langle - | - \rangle_{\mathbf{s}}|^2 = \frac{1 + \mathbf{r} \cdot \mathbf{s}}{2}, \\ |\mathbf{r}\langle + | - \rangle_{\mathbf{s}}|^2 &= |\mathbf{r}\langle - | + \rangle_{\mathbf{s}}|^2 = \frac{1 - \mathbf{r} \cdot \mathbf{s}}{2}. \end{aligned} \quad (26)$$

B. Graph basics

A graph $G(V, E)$ is specified by a vertex set V and edge set E , where each edge is a two-vertex subset of V (here we only consider graphs without loops) [71]. Two distinct vertices $j, k \in V$ are adjacent if $\{j, k\} \in E$, in which case j, k are also called neighbors. The degree of a vertex j is the number of its neighbors and is denoted by $\deg(j)$. The degree of G is the maximum vertex degree and is denoted by $\Delta(G)$. The graph G is k -regular if all the vertices have degree k . The graph G is connected if for any pair of distinct vertices i, j , there exists a sequence of vertices i_1, i_2, \dots, i_h with $i_1 = i$ and $i_h = j$ such that each pair of consecutive vertices are adjacent, that is, $\{i_k, i_{k+1}\} \in E$ for $k = 1, 2, \dots, h - 1$.

Two distinct edges of G are adjacent if they share a same vertex and nonadjacent otherwise. A *matching* M is a subset of E in which no two edges are adjacent. The matching is a *maximal matching* if it is not contained in any other matching; it is a *maximum matching* if it contains the largest number of edges. The *matching number* is the cardinality of a maximum matching and is denoted by $\nu(G)$. A *matching cover* \mathcal{M} is a set of matchings that covers the edge set E , which means $\cup_{M \in \mathcal{M}} M = E$. An *edge coloring* of G is an assignment of colors to its edge such that only nonadjacent edges can have the same color. An edge coloring is trivial if all edges have different colors. By definition, each edge coloring determines a matching cover composed of disjoint matchings, and vice versa. The *chromatic index* (or edge chromatic number) of G

is the minimum number of colors required to color the edges of G and is denoted by $\chi'(G)$. Meanwhile, $\chi'(G)$ is also the minimum number of matchings required to cover the edge set E . According to Vizing's theorem [71, 72], the chromatic index of G satisfies

$$\Delta(G) \leq \chi'(G) \leq \Delta(G) + 1. \quad (27)$$

C. AKLT Hamiltonians and AKLT States

Let $G(V, E)$ be a connected graph with n vertices, to define the AKLT Hamiltonian associated with this graph, we first assign a Hilbert space \mathcal{H}_j of dimension $\deg(j) + 1$ to each vertex j . The whole Hilbert space is a tensor product of \mathcal{H}_j , that is, $\mathcal{H} = \bigotimes_{j \in V} \mathcal{H}_j$. Then we can assign a spin operator $\mathbf{S}_j = (S_{j,x}, S_{j,y}, S_{j,z})$ of spin value $S_j = \deg(j)/2$ on \mathcal{H}_j . Next, for each edge $e = \{j, k\} \in E$ of the graph, define $S_e = S_j + S_k$, then S_e is the maximum possible value of the total spin of the two nodes. Define

$$S_E := \max_{e \in E} S_e = \max_{\{j, k\} \in E} (S_j + S_k); \quad (28)$$

then we have

$$S_E \leq \Delta(G), \quad (29)$$

where the inequality is saturated if G is regular.

Given an edge $e = \{j, k\}$, denote by $P_e = P_{S_e}(\mathbf{S}_j + \mathbf{S}_k)$ the projector onto the spin- S_e subspace of spins j and k . To be concrete, the projector can be expressed as follows,

$$P_e = P_{S_e}(\mathbf{S}_j + \mathbf{S}_k) = \prod_{l=|S_j - S_k|}^{S_j + S_k - 1} \frac{(\mathbf{S}_j + \mathbf{S}_k)^2 - l(l+1)}{S_e(S_e + 1) - l(l+1)}, \quad (30)$$

where

$$\begin{aligned} (\mathbf{S}_j + \mathbf{S}_k)^2 &= (S_{j,x} + S_{k,x})^2 + (S_{j,y} + S_{k,y})^2 \\ &\quad + (S_{j,z} + S_{k,z})^2. \end{aligned} \quad (31)$$

When $S_j = S_k = 1$, Eq. (30) can be simplified as

$$P_2(\mathbf{S}_j + \mathbf{S}_k) = \frac{\mathbf{S}_j \cdot \mathbf{S}_k}{2} + \frac{(\mathbf{S}_j \cdot \mathbf{S}_k)^2}{6} + \frac{1}{3}. \quad (32)$$

When $S_j = S_k = 3/2$, Eq. (30) can be simplified as

$$\begin{aligned} P_3(\mathbf{S}_i + \mathbf{S}_j) &= \frac{27}{160} \mathbf{S}_i \cdot \mathbf{S}_j + \frac{29}{360} (\mathbf{S}_i \cdot \mathbf{S}_j)^2 \\ &\quad + \frac{1}{90} (\mathbf{S}_i \cdot \mathbf{S}_j)^3 + \frac{11}{128}. \end{aligned} \quad (33)$$

Now the AKLT Hamiltonian associated with the graph $G(V, E)$ can be expressed as

$$H_G = \sum_{e \in E} P_e = \sum_{\{j, k\} \in E} P_{S_j + S_k}(\mathbf{S}_j + \mathbf{S}_k). \quad (34)$$

It is known that this Hamiltonian is frustration free and has a unique ground state [11–13], which is denoted by $|\Psi_G\rangle$ henceforth. By definition we have

$$P_e|\Psi_G\rangle = 0 \quad \forall e \in E. \quad (35)$$

Moreover, $|\Psi_G\rangle$ is the only state (up to an irrelevant overall phase factor) that satisfies this condition.

Suppose $e, e' \in E$ are two edges of G ; then P_e and $P_{e'}$ commute unless the intersection $e \cap e'$ is nonempty. Suppose $e = \{j, k\}$, then at most $\deg(j) + \deg(k) - 2$ projectors $P_{e'}$ do not commute with P_e . Let

$$\begin{aligned} g &= g(H_G) = \max_{j < k} [\deg(j) + \deg(k) - 2] = 2 \max_{e \in E} S_e - 2 \\ &= 2S_E - 2; \end{aligned} \quad (36)$$

then each projector P_e does not commute with at most g projectors that compose the Hamiltonian H_G in Eq. (34). By Eq. (29) we have

$$g \leq 2\Delta(G) - 2. \quad (37)$$

When G is the cycle graph with $n \geq 3$ vertices, we get the prototypical 1D AKLT Hamiltonian,

$$H^\circ(n) := H_G = \sum_{j=1}^n P_2(\mathbf{S}_j + \mathbf{S}_{j+1}), \quad (38)$$

where the vertex label $n+1$ is identified with 1 by convention. Explicit expression for the AKLT state $|\Psi_G\rangle$ is known [7, 8], but it is not necessary to the current study. By contrast, the AKLT Hamiltonian for the open chain with n nodes is denoted by

$$\begin{aligned} H_{\frac{1}{2}, \frac{1}{2}}(n) &:= P_{\frac{3}{2}}(\mathbf{S}_1 + \mathbf{S}_2) + P_{\frac{3}{2}}(\mathbf{S}_{n-1} + \mathbf{S}_n) \\ &\quad + \sum_{j=2}^{n-2} P_2(\mathbf{S}_j + \mathbf{S}_{j+1}); \end{aligned} \quad (39)$$

here the spin values for the two boundary spins are both equal to $1/2$ as indicated in the subscripts. For the convenience of later discussions, we also define two auxiliary Hamiltonians,

$$H_{\frac{1}{2}, 1}(n) := P_{\frac{3}{2}}(\mathbf{S}_1 + \mathbf{S}_2) + \sum_{j=2}^{n-1} P_2(\mathbf{S}_j + \mathbf{S}_{j+1}), \quad (40)$$

$$H_{1, 1}(n) := \sum_{j=1}^{n-1} P_2(\mathbf{S}_j + \mathbf{S}_{j+1}), \quad (41)$$

where the subscripts indicate the spin values of the two boundary spins. Note that the ground state spaces of $H_{\frac{1}{2}, 1}(n)$ and $H_{1, 1}(n)$ are two-fold degenerate and four-fold degenerate, respectively, in contrast with $H^\circ(n)$ and $H_{\frac{1}{2}, \frac{1}{2}}(n)$, which are nondegenerate.

D. Spectral gaps of AKLT Hamiltonians

The spectral gaps of AKLT Hamiltonians are of key interest in many-body physics. They also play a crucial role in the verification of AKLT states as we shall see later. In the original papers [7, 8], Affleck, Kennedy, Lieb, and Tasaki proved that the AKLT Hamiltonian on the closed chain is gapped. Recently, researchers further showed that the AKLT Hamiltonians on several 2D lattices are also gaped. Notably, spectral gaps can be established rigorously for the honeycomb lattice, decorated honeycomb lattice, and decorated square lattice [73–77]. The estimated spectral gaps for the 1D chain, honeycomb lattice, and square lattice are 0.350, 0.100, and 0.015, respectively [6, 78]. Here we discuss briefly about the spectral gaps in the 1D case and for arbitrary connected graphs up to five vertices. The spectral gap of the Hamiltonian H_G is denoted by $\gamma(H_G)$ or γ for simplicity when there is no danger of confusion.

1. 1D chains

The spectral gaps of the AKLT Hamiltonians for four types of 1D chains up to 10 nodes are presented in Table I and illustrated Fig. 1. Numerical calculation shows that the spectral gaps for open chains, corresponding to $H_{\frac{1}{2}, \frac{1}{2}}(n)$, $H_{\frac{1}{2}, 1}(n)$, and $H_{1, 1}(n)$, decrease monotonically with the number of nodes. In the case of the closed chain corresponding to $H^\circ(n)$, by contrast, the spectral gap decreases monotonically if the chain has odd length, but increases monotonically if the chain has even length. In addition, numerical calculation suggests the following relations,

$$\gamma(H_{\frac{1}{2}, \frac{1}{2}}(n)) \geq \gamma(H_{\frac{1}{2}, 1}(n)) \geq \gamma(H_{1, 1}(n)), \quad n \geq 3, \quad (42)$$

$$\gamma(H_{\frac{1}{2}, \frac{1}{2}}(n)) \geq \gamma(H^\circ(n)), \quad n \geq 4, n \neq 5. \quad (43)$$

In the thermodynamic limit, the AKLT Hamiltonian on the closed chain was shown to be gaped already in the original work of AKLT [7, 8]. Later, Knabe derived

TABLE I. Spectral gaps of the AKLT Hamiltonians $H_{\frac{1}{2}, \frac{1}{2}}(n)$, $H_{\frac{1}{2}, 1}(n)$, $H_{1, 1}(n)$, and $H^\circ(n)$ for $n = 3, 4, \dots, 10$ together with the lower bounds \tilde{c}_n and c_n defined in Theorems 1 and 2. Note that \tilde{c}_k is a lower bound for $\gamma(H^\circ(n))$ when $n > k$, while c_k is a lower bound for $\gamma(H^\circ(n))$ when $n > 2k$.

n	3	4	5	6	7	8	9	10
$H_{\frac{1}{2}, \frac{1}{2}}$	0.667	0.517	0.454	0.421	0.402	0.390	0.381	0.376
$H_{\frac{1}{2}, 1}$	0.592	0.473	0.431	0.408	0.393	0.384	0.377	0.372
$H_{1, 1}$	0.500	0.449	0.413	0.398	0.387	0.379	0.374	0.367
H°	0.833	0.333	0.454	0.348	0.402	0.350	0.381	0.350
\tilde{c}_n	0	0.173	0.218	0.248	0.264	0.276	0.284	0.291
c_n	0	0.207	0.254	0.280	0.290	0.296	0.299	0.301

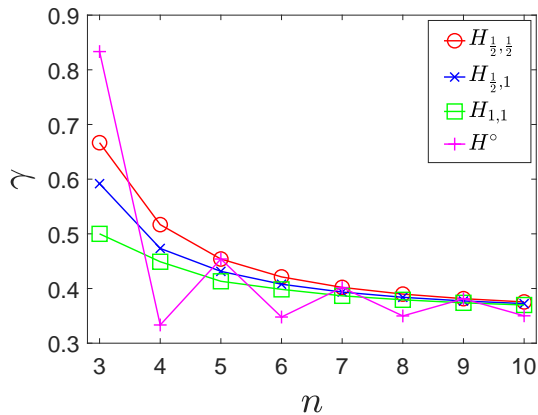


FIG. 1. Spectral gaps of the AKLT Hamiltonians $H_{\frac{1}{2}, \frac{1}{2}}(n)$, $H_{\frac{1}{2}, 1}(n)$, $H_{1,1}(n)$, and $H^\circ(n)$ for $n = 3, 4, \dots, 10$. Here lines are guides for the eyes (similarly for other figures).

a lower bound for $\gamma(H^\circ(n))$ based on the spectral gap $\gamma(H_{1,1}(k))$ [79], where $H_{1,1}(k)$ is the Hamiltonian associated with the open chain of k nodes as defined in Eq. (41).

Theorem 1 (Knabe). Suppose $n > k > 2$. Then $\gamma(H^\circ(n)) \geq \tilde{c}_k$ with

$$\tilde{c}_k := \left(\frac{k-1}{k-2} \right) \left[\gamma(H_{1,1}(k)) - \frac{1}{k-1} \right]. \quad (44)$$

The Knabe's bound above is nontrivial whenever $\gamma(H_{1,1}(k)) > 1/(k-1)$. Recently, Gosset and Mozgunov proved a stronger result as stated in the following theorem [80].

Theorem 2 (Gosset-Mozgunov). Suppose $k > 2$ and $n > 2k$. Then $\gamma(H^\circ(n)) \geq c_k$ with

$$c_k := \frac{5}{6} \left(\frac{k^2 + k}{k^2 - 4} \right) \left[\gamma(H_{1,1}(k)) - \frac{6}{k(k+1)} \right]. \quad (45)$$

Numerical calculation suggests that Theorems 1 and 2 still hold if $H^\circ(n)$ is replaced by $H_{\frac{1}{2}, \frac{1}{2}}(n)$, $H_{\frac{1}{2}, 1}(n)$, or $H_{1,1}(n)$ (cf. Table I).

2. general graphs

Next, we consider the spectral gaps of AKLT Hamiltonians associated with general connected graphs $G(V, E)$ up to five vertices, that is, $n = |V| \leq 5$. Up to isomorphism there are 1 connected graph of two vertices, 2 connected graphs of three vertices, 6 connected graphs of four vertices, and 21 connected graphs of five vertices. The corresponding spectral gaps are presented in Table V in Appendix D. Calculation shows that the Hamiltonian associated with the complete graph has the largest spectral gap among all graphs with the same number of vertices, as illustrated in Fig. 2. To be specific, the spectral

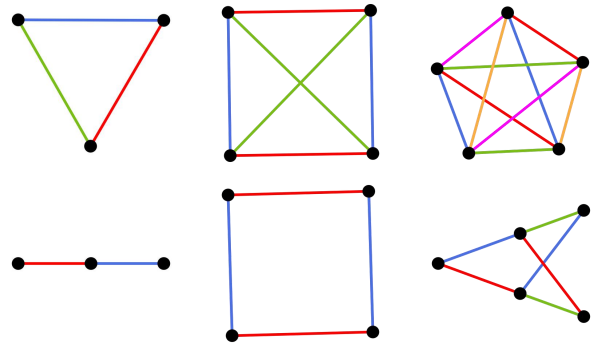


FIG. 2. Connected graphs of three, four, and five vertices whose AKLT Hamiltonians have the largest spectral gaps (up) and smallest spectral gaps (down).

gaps are $5/6$, $7/10$, and $3/5$ for complete graphs of three, four, and five vertices, respectively. We guess the same conclusion holds even for graphs with more than five vertices. We have not found a general pattern for the graph that leads to the smallest spectral gap: the minimum is attained at the linear graph when $n = 3$, the cycle graph when $n = 4$, and the lower-right graph shown in Fig. 2 (corresponding to graph No. 18 in Table V) when $n = 5$.

IV. BOND VERIFICATION PROTOCOLS

To verify the AKLT state associated with a given graph, we first need to construct bond verification protocols for verifying each pair of adjacent nodes, which is tied to the problem of subspace verification. Here we shall focus on verification protocols that build on spin measurements.

A. Test operators based on spin measurements

Let \mathcal{S}_1 and \mathcal{S}_2 be two spin operators of spin values S_1 and S_2 , respectively. Let $S = S_1 + S_2$ and let $P_S = P_S(\mathcal{S}_1 + \mathcal{S}_2)$ be the projector onto the subspace associated with the maximum total spin S as defined in Eq. (30); let $Q = 1 - P_S$. Here our goal is to verify the null space of P_S , that is, the support of Q . To this end, we shall construct test operators based on spin measurements.

Suppose the two parties perform spin measurements along directions \mathbf{r} , \mathbf{s} , respectively, where \mathbf{r} , \mathbf{s} are real unit vectors in dimension 3. The measurement outcomes can be labeled by eigenvalues m_1 and m_2 of $\mathbf{r} \cdot \mathcal{S}_1$ and $\mathbf{s} \cdot \mathcal{S}_2$, respectively. Let

$$|S_1, m_1; S_2, m_2\rangle_{\mathbf{r}, \mathbf{s}} := |S_1, m_1\rangle_{\mathbf{r}} \otimes |S_2, m_2\rangle_{\mathbf{s}}, \quad (46)$$

$$p_{\mathbf{r}, \mathbf{s}}(S_1, m_1; S_2, m_2) := \|P_S |S_1, m_1; S_2, m_2\rangle_{\mathbf{r}, \mathbf{s}}\|^2 = \text{tr}[P_S P_{\mathbf{r}, \mathbf{s}}(S_1, m_1; S_2, m_2)], \quad (47)$$

where $P_{\mathbf{r}, \mathbf{s}}(S_1, m_1; S_2, m_2)$ is the rank-1 projector onto

the state $|S_1, m_1; S_2, m_2\rangle_{\mathbf{r}, \mathbf{s}}$. Then a general test operator R is a linear combination of the projectors $P_{\mathbf{r}, \mathbf{s}}(S_1, m_1; S_2, m_2)$ associated with all possible outcomes. To guarantee that all states supported in the support of Q can pass the test with certainty, R should satisfy the condition

$$R \geq P_{\mathbf{r}, \mathbf{s}}(S_1, m_1; S_2, m_2) \quad (48)$$

whenever $p_{\mathbf{r}, \mathbf{s}}(S_1, m_1; S_2, m_2) < 1$.

If \mathbf{r} is neither parallel nor antiparallel to \mathbf{s} , then the inequality in Eq. (48) should hold for all possible outcomes m_1, m_2 according to Lemma 1 below. So the test operator R is equal to the identity operator, and the test is trivial. When \mathbf{s} is parallel to \mathbf{r} , nontrivial test operators can be constructed. Here we are particularly interested in the canonical test projector associated with \mathbf{r} as defined as follows,

$$\begin{aligned} R_{\mathbf{r}} &:= 1 - P_{\mathbf{r}}(S_1; S_2) - P_{\mathbf{r}}(-S_1; -S_2) \\ &= 1 - |++\rangle_{\mathbf{r}}\langle ++| - |--\rangle_{\mathbf{r}}\langle --|, \end{aligned} \quad (49)$$

where

$$P_{\mathbf{r}}(S_1; S_2) := P_{\mathbf{r}, \mathbf{r}}(S_1, S_1; S_2, S_2), \quad (50)$$

$$P_{\mathbf{r}}(-S_1; -S_2) := P_{\mathbf{r}, \mathbf{r}}(S_1, -S_1; S_2, -S_2), \quad (51)$$

$$|\pm \pm\rangle_{\mathbf{r}} := |\pm S_1\rangle_{\mathbf{r}} \otimes |\pm S_2\rangle_{\mathbf{r}}. \quad (52)$$

According to Lemma 1 below, any other test operator R based on the same spin measurements satisfy $R \geq R_{\mathbf{r}}$ and is thus suboptimal. When $\mathbf{s} = -\mathbf{r}$, the set of accessible test operators does not change given that

$$P_{\mathbf{r}, \mathbf{s}}(S_1, m_1; S_2, m_2) = P_{\mathbf{r}, -\mathbf{s}}(S_1, m_1; S_2, -m_2). \quad (53)$$

Therefore, it suffices to consider canonical test projectors based on parallel spin measurements.

The following lemma employed in the above analysis is proved in Appendix A.

Lemma 1. Suppose S_1 and S_2 are positive integers or half integers. Then

$$p_{\mathbf{r}, \mathbf{s}}(S_1, m_1; S_2, m_2) \leq 1, \quad (54)$$

and the inequality is saturated iff one of the following four conditions holds

$$\mathbf{r} = \mathbf{s}, \quad m_1 = S_1, \quad m_2 = S_2; \quad (55a)$$

$$\mathbf{r} = \mathbf{s}, \quad m_1 = -S_1, \quad m_2 = -S_2; \quad (55b)$$

$$\mathbf{r} = -\mathbf{s}, \quad m_1 = S_1, \quad m_2 = -S_2; \quad (55c)$$

$$\mathbf{r} = -\mathbf{s}, \quad m_1 = -S_1, \quad m_2 = S_2. \quad (55d)$$

B. Spectral gaps of bond verification protocols

According to the discussion in Sec. IV A, each canonical test projector is specified by a unit vector \mathbf{r} in dimension 3. Given any probability distribution μ on the

unit sphere, then a bond verification protocol can be constructed by performing each test $R_{\mathbf{r}}$ with a suitable probability. The corresponding verification operator reads

$$\Omega_{S_1, S_2}(\mu) = \int R_{\mathbf{r}} d\mu(\mathbf{r}). \quad (56)$$

When S_1 and S_2 are clear from the context, $\Omega_{S_1, S_2}(\mu)$ can be abbreviated as $\Omega(\mu)$ for simplicity. The spectral gap of $\Omega_{S_1, S_2}(\mu)$ reads

$$\nu(\Omega_{S_1, S_2}(\mu)) = 1 - \|P_S \Omega_{S_1, S_2}(\mu) P_S\|, \quad (57)$$

where P_S is the projector defined according to Eq. (30). Note that the spectral gap $\nu(\Omega_{S_1, S_2}(\mu))$ is invariant when μ is subjected to any orthogonal transformation; in addition, $\nu(\Omega(\mu))$ is concave in μ .

Lemma 2. The spectral gap $\nu(\Omega_{S_1, S_2}(\mu))$ is independent of S_1 and S_2 once the sum $S = S_1 + S_2$ is fixed.

Lemma 2 follows from the definition of the test operator $R_{\mathbf{r}}$ in Eq. (49) and the fact that the representation of the angular momentum operators carried by the states $|S_1, S_2\rangle_{\mathbf{r}}$ is independent of S_1 and S_2 once the sum $S = S_1 + S_2$ is fixed. This result holds even if $S_1 = 0$ or $S_2 = 0$, which is very helpful to simplify the computation of the spectral gap. In view of these facts, we shall denote the spectral gap of $\Omega_{S_1, S_2}(\mu)$ by $\nu_S(\mu)$ for simplicity.

Denote by μ_{sym} the average distribution of μ and its center inversion. Define

$$\begin{aligned} \Omega_S(\mu) &:= \int (1 - |S\rangle_{\mathbf{r}}\langle S| - |-S\rangle_{\mathbf{r}}\langle -S|) d\mu(\mathbf{r}) \\ &= 1 - 2 \int |S\rangle_{\mathbf{r}}\langle S| d\mu_{\text{sym}}(\mathbf{r}). \end{aligned} \quad (58)$$

Then

$$\nu_S(\mu) = 1 - \|\Omega_S(\mu)\| = \lambda_{\min}(O_S(\mu)), \quad (59)$$

where

$$O_S(\mu) := 2 \int |S\rangle_{\mathbf{r}}\langle S| d\mu_{\text{sym}}(\mathbf{r}), \quad (60)$$

and λ_{\min} denotes the smallest eigenvalue. In particular, $\nu_S(\mu)$ is nonzero iff the operator $O_S(\mu)$ has full rank. When μ is a discrete distribution, to achieve a nonzero spectral gap $\nu_S(\mu) > 0$, the support of μ_{sym} should contain at least $2S + 1$ points, so the support of μ should contain at least $\lceil S + \frac{1}{2} \rceil$ points. To construct a nontrivial bond verification protocol, therefore, at least $\lceil S + \frac{1}{2} \rceil$ distinct canonical tests are required.

The following lemma proved in Appendix B is very instructive to understanding the properties of $\nu_S(\mu)$.

Lemma 3. Suppose μ is a probability distribution on the unit sphere. Then $\nu_S(\mu)$ is nonincreasing in S . If $S_1 \leq S_2$, then

$$\nu_{S_1}(\mu) \geq \frac{2S_2 + 1}{2S_1 + 1} \nu_{S_2}(\mu). \quad (61)$$

In the special case $S = 1/2$, we have $\nu_S(\mu) = 1$ irrespective of the distribution μ . So Lemma 3 implies that

$$\nu_S(\mu) \leq \frac{2}{2S+1}, \quad (62)$$

which sets an upper bound for the spectral gap achievable by spin measurements. Alternatively, Eq. (62) follows from Eq. (58), which implies that

$$\text{tr}[\Omega_S(\mu)] = 2S - 1, \quad \|\Omega_S(\mu)\| \geq \frac{2S-1}{2S+1}. \quad (63)$$

Bond verification protocols that saturate the upper bound in Eq. (62) are called optimal. Notably, this bound is saturated when μ is the isotropic (uniform) distribution on the unit sphere, which leads to the *isotropic protocol*.

To clarify the condition required for constructing an optimal bond verification protocol, we need to introduce additional concepts. Let t be a nonnegative integer. A probability distribution μ on the unit sphere is a (spherical) t -design if the average of any polynomial of degree less than or equal to t over the distribution is equal to the average over the isotropic distribution [81–83]. By definition a t -design is automatically a $(t-1)$ -design for any positive integer t . The design strength of the distribution μ is the largest integer t such that μ is a t -design. The isotropic distribution forms a spherical ∞ -design and has strength ∞ . If μ is center symmetric, then μ is a $2j$ -design iff μ is a $(2j+1)$ -design for any positive integer j , so the strength of μ is always an odd integer. The next theorem follows from a similar reasoning used to establish Theorem 3 in the companion paper [69]. A self-contained proof is presented in Appendix C.

Theorem 3. Let μ be a probability distribution on the unit sphere and S a positive integer or half integer. Then the following four statements are equivalent.

1. $\nu_S(\mu) = \frac{2}{2S+1}$.
2. $\Omega_S(\mu) = \frac{2S-1}{2S+1}$.
3. $\Omega_S(\mu)$ is proportional to the identity operator.
4. μ_{sym} forms a spherical t -design with $t = 2S$.

According to the discussion before Theorem 3, when S is a positive integer, μ_{sym} forms a $2S$ -design iff it forms a $(2S+1)$ -design; when S is a positive half integer, μ_{sym} forms a $2S$ -design iff it forms a $2\lfloor S \rfloor$ -design.

C. Concrete verification protocols

In this section we construct a number of concrete bond verification protocols based on discrete distributions on the unit sphere, which are appealing to practical applications.

First, we consider bond verification protocols based on platonic solids. Each platonic solid inscribed in the unit

sphere determines a probability distribution on the unit sphere (by convention all vertices have the same weight), which in turn determines a bond verification protocol for any given pair of spins. In this way we can construct five bond verification protocols by virtue of the five platonic solids. To be concrete, the vertices of the regular tetrahedron are chosen to be:

$$\begin{aligned} & \frac{1}{\sqrt{3}}(1, 1, 1), & \frac{1}{\sqrt{3}}(1, -1, -1), \\ & \frac{1}{\sqrt{3}}(-1, 1, -1), & \frac{1}{\sqrt{3}}(-1, -1, 1). \end{aligned} \quad (64)$$

The vertices of the octahedron are chosen to be:

$$(\pm 1, 0, 0), (0, \pm 1, 0), (0, 0, \pm 1). \quad (65)$$

The vertices of the cube are chosen to be:

$$\frac{1}{\sqrt{3}}(\pm 1, \pm 1, \pm 1). \quad (66)$$

The vertices of the icosahedron are chosen to be:

$$\begin{aligned} & \frac{1}{\sqrt{1+b^2}}(\pm 1, \pm b, 0), & \frac{1}{\sqrt{1+b^2}}(\pm b, 0, \pm 1), \\ & \frac{1}{\sqrt{1+b^2}}(0, \pm 1, \pm b), \end{aligned} \quad (67)$$

where $b = (1 + \sqrt{5})/2$. The vertices of the dodecahedron are chosen to be:

$$\begin{aligned} & \frac{1}{\sqrt{3}}\left(\pm b, \pm \frac{1}{b}, 0\right), & \frac{1}{\sqrt{3}}\left(\pm \frac{1}{b}, 0, \pm b\right), \\ & \frac{1}{\sqrt{3}}\left(0, \pm b, \pm \frac{1}{b}\right), & \frac{1}{\sqrt{3}}(\pm 1, \pm 1, \pm 1). \end{aligned} \quad (68)$$

For the convenience of the following discussions, the verification operators associated with the regular tetrahedron, octahedron, cube, icosahedron, and dodecahedron, are denoted by Ω_t , Ω_o , Ω_c , Ω_i , and Ω_d , respectively. Although these verification operators may depend on the specific choices of vertices, their spectral gaps as shown in Table II are independent of the specific choices. Except for the regular tetrahedron, every platonic solid is center symmetric, and the two tests based on each pair of antipodal vertices are equivalent; so the total number of distinct tests is equal to one half of the vertex number. It is known that the regular tetrahedron, octahedron, cube, icosahedron, and dodecahedron form spherical t -designs with $t = 2, 3, 3, 5, 5$, respectively. Therefore, the icosahedron and dodecahedron protocols are optimal when $S = S_1 + S_2 \leq 5/2$.

To construct optimal bond verification protocols for $S \geq 3$, we need to go beyond platonic solids and consider spherical designs with higher strengths. For example, a spherical 7-design can be constructed from an orbit of the rotational symmetry group of the standard cube (which has order 24): one fiducial vector has the form

TABLE II. Spectral gaps $\nu_S(\mu)$ for $1 \leq S \leq 4$ of bond verification protocols based on platonic solids, μ_{24} , μ_{32} , and the isotropic distribution. Vertex number, distinct test number, and design strength of each distribution are also shown for completeness.

Protocol	Ω	Vertex number	Test number	design strength	ν_1	$\nu_{3/2}$	ν_2	$\nu_{5/2}$	ν_3	$\nu_{7/2}$	ν_4
Tetrahedron	Ω_t	4	4	2	$\frac{2}{3}$	$\frac{1}{2}$	$\frac{1}{3}$	$\frac{5}{18}$	$\frac{5}{27}$	$\frac{5}{54}$	0
Octahedron	Ω_o	6	3	3	$\frac{2}{3}$	$\frac{1}{2}$	$\frac{1}{3}$	$\frac{1}{6}$	0	0	0
Cube	Ω_c	8	4	3	$\frac{2}{3}$	$\frac{1}{2}$	$\frac{1}{3}$	$\frac{5}{18}$	$\frac{5}{27}$	$\frac{5}{54}$	0
Icosahedron	Ω_i	12	6	5	$\frac{2}{3}$	$\frac{1}{2}$	$\frac{2}{5}$	$\frac{1}{3}$	$\frac{4}{15}$	$\frac{7}{30}$	$\frac{14}{75}$
Dodecahedron	Ω_d	20	10	5	$\frac{2}{3}$	$\frac{1}{2}$	$\frac{2}{5}$	$\frac{1}{3}$	$\frac{5}{18}$	$\frac{2}{9}$	$\frac{16}{81}$
μ_{24}	$\Omega(\mu_{24})$	24	24	7	$\frac{2}{3}$	$\frac{1}{2}$	$\frac{2}{5}$	$\frac{1}{3}$	$\frac{2}{7}$	$\frac{1}{4}$	$\frac{23}{105}$
μ_{32}	$\Omega(\mu_{32})$	32	16	9	$\frac{2}{3}$	$\frac{1}{2}$	$\frac{2}{5}$	$\frac{1}{3}$	$\frac{2}{7}$	$\frac{1}{4}$	$\frac{2}{9}$
Isotropic	Ω_{iso}	∞	∞	∞	$\frac{2}{3}$	$\frac{1}{2}$	$\frac{2}{5}$	$\frac{1}{3}$	$\frac{2}{7}$	$\frac{1}{4}$	$\frac{2}{9}$

(u_1, u_2, u_3) , where

$$u_j = \sqrt{\frac{1}{3} \left(1 + 2\sqrt{\frac{2}{5}} \cos \frac{\theta + 2j\pi}{3} \right)}, \quad \theta = \arctan \frac{3\sqrt{10}}{20} \quad (69)$$

for $j = 1, 2, 3$. This orbit has 24 vectors, which can be expressed as

$$\{(a_1 u_{\sigma(1)}, a_2 u_{\sigma(2)}, a_1 a_2 \text{sgn}(\sigma) u_{\sigma(3)}) | a_1, a_2 = \pm 1, \sigma \in \mathcal{S}_3\}. \quad (70)$$

Here \mathcal{S}_3 denotes the symmetric group of three letters; $\text{sgn}(\sigma)$ is equal to 1 for even permutations and equal to -1 for odd permutations. All points corresponding to these vectors have the same weight as before; the resulting distribution on the unit sphere is denoted by μ_{24} henceforth. Note that μ_{24} is not center symmetric.

A spherical 9-design can be constructed from the union of the vertices of the icosahedron in Eq. (67) and that of the dodecahedron in Eq. (68), which form pentakis dodecahedron (cf. Ref. [84]). The icosahedron has weight $5/14$ in total and each vertex has weight $5/168$, while the dodecahedron has weight $9/14$ in total and each vertex has weight $9/280$. The resulting distribution on the unit sphere is denoted by μ_{32} , which is center symmetric by construction. The spectral gaps $\nu_S(\mu)$ for $1 \leq S \leq 4$ of bond verification operators based on μ_{24} and μ_{32} are also shown in Table II.

V. VERIFICATION OF AKLT STATES: GENERAL APPROACH

A. Construction of verification protocols

Consider the AKLT Hamiltonian H_G and AKLT state $|\Psi_G\rangle$ associated with a given graph $G = (V, E)$ of n vertices [cf. Eqs. (34) and (35)]. To verify $|\Psi_G\rangle$, we need to verify each bond associated with each edge of the graph G . More specifically, we need to verify the null space of the projector P_e for each $e \in E$. Here we shall focus on

bond verification protocols based on spin measurements, which are determined by probability distributions on the unit sphere as discussed in Sec. IV. For simplicity we also assume that the same distribution is chosen for each bond, although this is not compulsory.

Let μ be a probability distribution on the unit sphere. According to Sec. IV we can construct a bond verification protocol for each edge of the graph G . The bond verification operator associated with the edge $e \in E$ is denoted by $\Omega_e(\mu)$ [cf. Eq. (56)]. Given a matching M of G , then a test for $|\Psi_G\rangle$ can be constructed by performing the bond verification protocols for all the bonds associated with edges in M independently. The corresponding test operator is given by

$$T_M(\mu) = \prod_{e \in M} \Omega_e(\mu). \quad (71)$$

Note that all the bond verification operators $\Omega_e(\mu)$ for $e \in M$ commute with each other, so the order in the above product is irrelevant. Suppose $\nu(\Omega_e(\mu)) > 0$ for each $e \in M$, then a quantum state $|\Phi\rangle$ satisfies the condition $T_M|\Phi\rangle = |\Phi\rangle$ iff $P_e|\Phi\rangle = 0$ for each $e \in M$. Therefore, a state can pass the test $T_M(\mu)$ with certainty iff it belongs to the null space of the projector P_e for each $e \in M$. Let M' be another matching of G , then we can deduce from Eq. (71) the following relation:

$$T_M(\mu) \geq T_{M'}(\mu) \quad \text{if } M \subseteq M'. \quad (72)$$

Let $\mathcal{M} = \{M_1, M_2, \dots, M_m\}$ be a matching cover of G that consists of m matchings and let $p = (p_1, p_2, \dots, p_m)$ be a probability distribution on \mathcal{M} (we shall assume that the distribution is uniform when p is not mentioned explicitly). Then a verification protocol for $|\Psi_G\rangle$ can be constructed by performing each test $T_{M_l}(\mu)$ with probability p_l . The resulting verification protocol is specified by the triple (μ, \mathcal{M}, p) (here p can be omitted for the uniform distribution), and the corresponding verification operator reads

$$\Omega(\mu, \mathcal{M}, p) = \sum_{l=1}^m p_l T_{M_l}(\mu). \quad (73)$$

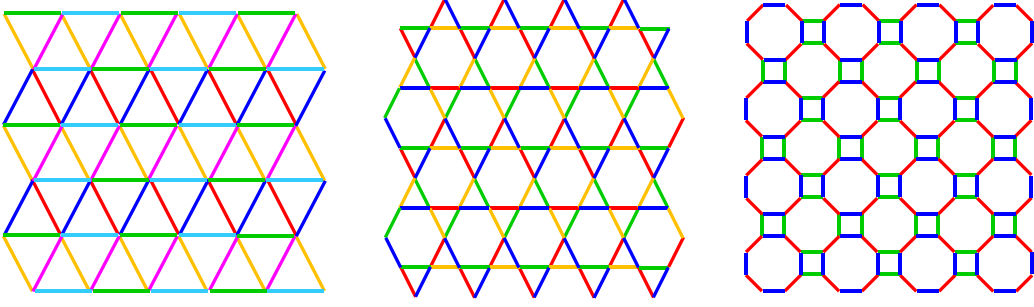


FIG. 3. Optimal edge colorings of several common 2D lattices: triangular lattice, kagome lattice, and square-octagon lattice. These optimal colorings can be used to construct efficient protocols for verifying AKLT states on these lattices, which require constant sample costs that are independent of the lattice size.

Suppose $p_l > 0$ for $l = 1, 2, \dots, m$ and $\nu(\Omega_e(\mu)) > 0$ for each $e \in \cup_l M_l = E$; then a quantum state $|\Phi\rangle$ can pass all the tests with certainty iff $P_e|\Phi\rangle = 0$ for each $e \in E$. So only the target state $|\Psi_G\rangle$ can pass all the tests with certainty, which means this verification protocol is effective. According to Eq. (72), the spectral gap of $\Omega(\mu, \mathcal{M}, p)$ does not decrease if M_l is replaced by another matching M'_l that contains M_l . To maximize the spectral gap, therefore, it is advisable to choose matching covers composed of maximal matchings.

If the matchings in $\mathcal{M} = \{M_1, M_2, \dots, M_m\}$ form one orbit under the symmetry group of the graph G , then the spectral gap of the verification operator $\Omega(\mu, \mathcal{M}, p)$ is maximized when the probability distribution p is uniform. In general, given the distribution μ and the matching cover \mathcal{M} , the maximum spectral gap of $\Omega(\mu, \mathcal{M}, p)$ can be determined by semidefinite programming (SDP). Define

$$\bar{T}_{M_l}(\mu) := T_{M_l}(\mu) - |\Psi_G\rangle\langle\Psi_G|, \quad (74)$$

$$\bar{\Omega}(\mu, \mathcal{M}, p) := \Omega(\mu, \mathcal{M}, p) - |\Psi_G\rangle\langle\Psi_G| = \sum_{l=1}^m p_l \bar{T}_{M_l}(\mu); \quad (75)$$

then

$$\nu(\Omega(\mu, \mathcal{M}, p)) = 1 - \|\bar{\Omega}(\mu, \mathcal{M}, p)\|. \quad (76)$$

To maximize the spectral gap of $\Omega(\mu, \mathcal{M}, p)$, it is equivalent to minimize the operator norm of $\bar{\Omega}(\mu, \mathcal{M}, p)$, which can be realized by the following SDP:

$$\begin{aligned} & \text{minimize} && h \\ & \text{subject to} && h \geq \sum_{l=1}^m p_l \bar{T}_{M_l}(\mu), \\ & && p_l \geq 0, \quad \sum_{l=1}^m p_l = 1. \end{aligned} \quad (77)$$

To construct an optimal matching protocol, in principle we need to consider all maximal matchings before

the optimization, which is feasible only for small systems. When this approach is too prohibitive, we can consider simple matching protocols and resort to analytical bounds derived in the next subsection.

B. Sample complexity

Before presenting our main results on the sample complexity, we need to introduce some terminology. Suppose P_e and $P_{e'}$ are two projectors associated with two edges of $G = (V, E)$ as defined in Eq. (30). Denote by $s(P_e P_{e'})$ the largest singular value of $P_e P_{e'}$ that is not equal to 1. By definition $s(P_e P_{e'}) = 0$ if $e = e'$ or if e and e' are disjoint. If $e = \{1, 2\}$ and $e' = \{2, 3\}$, then

$$P_e = P_{12} := P_{S_1+S_2}(\mathbf{S}_1 + \mathbf{S}_2), \quad (78)$$

$$P_{e'} = P_{23} := P_{S_2+S_3}(\mathbf{S}_2 + \mathbf{S}_3). \quad (79)$$

So the value of $s(P_e P_{e'}) = s(P_{12} P_{23})$ is determined by the spin values S_1, S_2, S_3 ; in addition, this value is invariant if S_1 and S_3 are exchanged. The specific value of $s^2(P_{12} P_{23})$ for $S_1, S_2, S_3 \leq 5/2$ can be found in Table III, which suggests the following conjecture.

Conjecture 1. Suppose S_1, S_2, S_3 are positive integers or half integers; then $s^2(P_{12} P_{23})$ is a rational number. If in addition $S_1, S_3 \leq S_2$, then

$$s^2(P_{12} P_{23}) \leq 1/4, \quad (80)$$

and the inequality is saturated iff $S_1 = S_2 = S_3$.

Define

$$s(G) := \max_{e, e' \in E} s(P_e P_{e'}) = \max_{e, e' \in E | e \neq e'} s(P_e P_{e'}). \quad (81)$$

By definition $0 \leq s(G) < 1$. Here $s(G)$ can be abbreviated as s if there is no danger of confusion. According to Table III, we have $s(G) = 1/2$ for most lattices of practical interest, including the open chain (with at least four nodes), closed chain, square lattice, honeycomb

TABLE III. Value of $s^2(P_{12}P_{23})$ with $P_{12} = P_{S_1+S_2}(\mathbf{S}_1 + \mathbf{S}_2)$ and $P_{23} = P_{S_2+S_3}(\mathbf{S}_2 + \mathbf{S}_3)$, where $s(P_{12}P_{23})$ is the largest singular value of $P_{12}P_{23}$ that is not equal to 1, and $s^2(P_{12}P_{23})$ is the largest eigenvalue of $P_{12}P_{23}P_{12}$ that is not equal to 1.

(S_1, S_3) \ S_2	$\frac{1}{2}$	1	$\frac{3}{2}$	2	$\frac{5}{2}$	3
$(\frac{1}{2}, \frac{1}{2})$	$\frac{1}{4}$	$\frac{1}{9}$	$\frac{1}{16}$	$\frac{1}{25}$	$\frac{1}{36}$	$\frac{1}{49}$
$(\frac{1}{2}, 1)$	$\frac{1}{3}$	$\frac{1}{6}$	$\frac{1}{10}$	$\frac{1}{15}$	$\frac{1}{21}$	$\frac{1}{28}$
$(\frac{1}{2}, \frac{3}{2})$	$\frac{3}{8}$	$\frac{1}{5}$	$\frac{1}{8}$	$\frac{3}{35}$	$\frac{1}{16}$	$\frac{1}{21}$
$(\frac{1}{2}, 2)$	$\frac{2}{5}$	$\frac{2}{9}$	$\frac{1}{7}$	$\frac{1}{10}$	$\frac{2}{27}$	$\frac{2}{35}$
$(\frac{1}{2}, \frac{5}{2})$	$\frac{5}{12}$	$\frac{5}{21}$	$\frac{5}{32}$	$\frac{1}{9}$	$\frac{1}{12}$	$\frac{5}{77}$
$(\frac{1}{2}, 3)$	$\frac{3}{7}$	$\frac{1}{4}$	$\frac{1}{6}$	$\frac{3}{25}$	$\frac{1}{11}$	$\frac{1}{14}$
$(1, 1)$	$\frac{4}{9}$	$\frac{1}{4}$	$\frac{4}{25}$	$\frac{1}{9}$	$\frac{4}{49}$	$\frac{1}{16}$
$(1, \frac{3}{2})$	$\frac{1}{2}$	$\frac{3}{10}$	$\frac{1}{5}$	$\frac{1}{7}$	$\frac{3}{28}$	$\frac{1}{12}$
$(1, 2)$	$\frac{8}{15}$	$\frac{1}{3}$	$\frac{8}{35}$	$\frac{1}{6}$	$\frac{8}{63}$	$\frac{1}{10}$
$(1, \frac{5}{2})$	$\frac{5}{9}$	$\frac{5}{14}$	$\frac{1}{4}$	$\frac{5}{27}$	$\frac{1}{7}$	$\frac{5}{44}$
$(1, 3)$	$\frac{4}{7}$	$\frac{3}{8}$	$\frac{4}{15}$	$\frac{1}{5}$	$\frac{12}{77}$	$\frac{1}{8}$
$(\frac{3}{2}, \frac{3}{2})$	$\frac{9}{16}$	$\frac{9}{25}$	$\frac{1}{4}$	$\frac{9}{49}$	$\frac{9}{64}$	$\frac{1}{9}$
$(\frac{3}{2}, 2)$	$\frac{3}{5}$	$\frac{2}{5}$	$\frac{2}{7}$	$\frac{3}{14}$	$\frac{1}{6}$	$\frac{2}{15}$
$(\frac{3}{2}, \frac{5}{2})$	$\frac{5}{8}$	$\frac{3}{7}$	$\frac{5}{16}$	$\frac{5}{21}$	$\frac{3}{16}$	$\frac{5}{33}$
$(\frac{3}{2}, 3)$	$\frac{9}{14}$	$\frac{9}{20}$	$\frac{1}{3}$	$\frac{9}{35}$	$\frac{9}{44}$	$\frac{1}{6}$
$(2, 2)$	$\frac{16}{25}$	$\frac{4}{9}$	$\frac{16}{49}$	$\frac{1}{4}$	$\frac{16}{81}$	$\frac{4}{25}$
$(2, \frac{5}{2})$	$\frac{2}{3}$	$\frac{10}{21}$	$\frac{5}{14}$	$\frac{5}{18}$	$\frac{2}{9}$	$\frac{2}{11}$
$(2, 3)$	$\frac{24}{35}$	$\frac{1}{2}$	$\frac{8}{21}$	$\frac{3}{10}$	$\frac{8}{33}$	$\frac{1}{5}$
$(\frac{5}{2}, \frac{5}{2})$	$\frac{25}{36}$	$\frac{25}{49}$	$\frac{25}{64}$	$\frac{25}{81}$	$\frac{1}{4}$	$\frac{25}{121}$
$(\frac{5}{2}, 3)$	$\frac{5}{7}$	$\frac{15}{28}$	$\frac{5}{12}$	$\frac{1}{3}$	$\frac{3}{11}$	$\frac{5}{22}$
$(3, 3)$	$\frac{36}{49}$	$\frac{9}{16}$	$\frac{4}{9}$	$\frac{9}{25}$	$\frac{36}{121}$	$\frac{1}{4}$

lattice, triangular lattice, kagome lattice, and square-octagon lattice (cf. Fig. 3). For the open chain with three nodes, we have $s(G) = 1/3$.

In the following theorem, $\gamma = \gamma(H_G)$ is the spectral gap of H_G , while S_E and $\nu_{S_E}(\mu)$ are defined in Eqs. (28) and (59), respectively.

Theorem 4. Let $|\Psi_G\rangle$ be the AKLT state defined on the graph $G = (V, E)$. Suppose $\Omega(\mu, \mathcal{M})$ is the verification operator specified by the probability distribution μ and the matching cover \mathcal{M} composed of m matchings. Then

$$\nu(\Omega(\mu, \mathcal{M})) \geq \frac{\nu_{S_E}(\mu)}{m} f\left(\frac{\gamma}{s^2 g^2}\right) \geq \frac{\nu_{S_E}(\mu)\gamma}{24m(S_E - 1)^2}, \quad (82)$$

where $s = s(G)$, $g = 2S_E - 2$, and

$$f(x) = \begin{cases} \frac{\sqrt{1+x}-1}{\sqrt{1+x}} & m = 2, \\ \frac{\sqrt{1+x}-1}{\sqrt{1+x}+1} & m \geq 3. \end{cases} \quad (83)$$

If μ_{sym} forms a spherical t -design with $t = 2S_E$, then

$$\begin{aligned} \nu(\Omega(\mu, \mathcal{M})) &\geq \frac{2}{m(2S_E + 1)} f\left(\frac{\gamma}{s^2 g^2}\right) \\ &\geq \frac{\gamma}{12m(2S_E + 1)(S_E - 1)^2}. \end{aligned} \quad (84)$$

Theorem 4 follows from Theorem 1 in the companion paper [69] as well as Lemma 3 and Theorem 3 in Sec. IV. In conjunction with Eq. (5), it is now straightforward to derive the following upper bound on the the minimum number of tests required to verify the AKLT state $|\Psi_G\rangle$ within infidelity ϵ and significance level δ :

$$\begin{aligned} N &\leq \left\lceil \frac{m(2S_E + 1) \ln(\delta^{-1})}{2\epsilon f\left(\frac{\gamma}{s^2 g^2}\right)} \right\rceil \\ &\leq \left\lceil \frac{12m(2S_E + 1)(S_E - 1)^2 \ln(\delta^{-1})}{\gamma\epsilon} \right\rceil. \end{aligned} \quad (85)$$

When $x \ll 1$, $f(x)$ can be approximated by $x/2$ for $m = 2$ and $x/4$ for $m \geq 3$. If $\gamma/(s^2 g^2) \ll 1$, then Eq. (82) implies that

$$\nu(\Omega(\mu, \mathcal{M})) \gtrsim \begin{cases} \frac{\gamma \nu_{S_E}(\mu)}{2m s^2 g^2} & m = 2, \\ \frac{\gamma \nu_{S_E}(\mu)}{4m s^2 g^2} & m \geq 3. \end{cases} \quad (86)$$

This equation is instructive to understanding the efficiency of the matching protocol. Equations (84) and (85) can be simplified in a similar way.

Recall that the minimum number of matchings required to cover the edge set of G is equal to the chromatic index $\chi'(G)$. If $m = \chi'(G)$, then Eq. (82) reduces to

$$\begin{aligned} \nu(\Omega(\mu, \mathcal{M})) &\geq \frac{\nu_{S_E}(\mu)}{\chi'(G)} f\left(\frac{\gamma}{s^2 g^2}\right) \geq \frac{\nu_{S_E}(\mu)\gamma}{24\chi'(G)(S_E - 1)^2} \\ &\geq \frac{\nu_{S_E}(\mu)\gamma}{24[\Delta(G) + 1][\Delta(G) - 1]^2} \geq \frac{\nu_{S_E}(\mu)\gamma}{24\Delta(G)^3}, \end{aligned} \quad (87)$$

where the third inequality follows from the facts that $\chi'(G) \leq \Delta(G) + 1$ and $S_E \leq \Delta(G)$. Although it is not always easy to find an optimal matching cover, a nearly optimal matching cover composed of $\chi'(G) + 1$ matchings can be found efficiently.

If in addition μ forms a spherical t -design with $t = 2S_E$, then Eq. (84) implies that

$$\begin{aligned} \nu(\Omega(\mu, \mathcal{M})) &\geq \frac{2}{\chi'(G)(2S_E + 1)} f\left(\frac{\gamma}{s^2 g^2}\right) \\ &\geq \frac{\gamma}{12\chi'(G)(2S_E + 1)(S_E - 1)^2} \geq \frac{\gamma}{24\Delta(G)^4}, \end{aligned} \quad (88)$$

Accordingly, Eq. (85) reduces to

$$N \leq \left\lceil \frac{\chi'(G)(2S_E + 1) \ln(\delta^{-1})}{2\epsilon f\left(\frac{\gamma}{s^2 g^2}\right)} \right\rceil \leq \left\lceil \frac{24\Delta(G)^4 \ln(\delta^{-1})}{\gamma\epsilon} \right\rceil. \quad (89)$$

For most AKLT states of practical interest, including those defined on various lattices as illustrated in Fig. 3

(see also Fig. 1 in the companion paper [69]), $\Delta(G)$ does not increase with the system size. So these AKLT states can be verified with constant sample cost that is independent of the system size as long as the spectral gap γ has a nontrivial system-independent lower bound. Our verification protocols are much more efficient than protocols known in the literature [33, 35, 37, 68] and the sample costs have much better scaling behaviors with respect to the system size, spectral gap of the underlying Hamiltonian, and the precision as quantified by the infidelity.

The next theorem follows from Theorems 2, 3 in the companion paper [69] and Lemma 3 in Sec. IV.

Theorem 5. Suppose \mathcal{M} in Theorem 4 is an edge coloring of G and let $p = (|M_1|, |M_2|, \dots, |M_m|)/|E|$; then

$$\nu(\Omega(\mu, \mathcal{M}, p)) \geq \frac{\nu_{S_E}(\mu)\gamma}{|E|} \geq \frac{2\nu_{S_E}(\mu)\gamma}{n(n-1)}. \quad (90)$$

If μ_{sym} forms a spherical t -design with $t = 2S_E$, then

$$\nu(\Omega(\mu, \mathcal{M}, p)) \geq \frac{2\gamma}{(2S_E + 1)|E|} \geq \frac{4\gamma}{(2S_E + 1)n(n-1)}. \quad (91)$$

The first inequality in Eq. (91) is saturated if S_e is independent of $e \in E$ and \mathcal{M} is the trivial edge coloring with $|\mathcal{M}| = |E|$.

By virtue of Eqs. (5) and (91), we can derive another upper bound on the minimum number of tests required to verify the AKLT state $|\Psi_G\rangle$ within infidelity ϵ and significance level δ :

$$N \leq \left\lceil \frac{(2S_E + 1)|E| \ln(\delta^{-1})}{2\gamma\epsilon} \right\rceil. \quad (92)$$

When G is a connected k -regular graph with $n \geq 2$ vertices, we have $|E| = nk/2$ and $S_e = S_E = \Delta(G) = k$ for all $e \in E$, so Eq. (90) reduces to

$$\nu(\Omega(\mu, \mathcal{M}, p)) \geq \frac{2\nu_k(\mu)\gamma}{nk}. \quad (93)$$

If in addition μ_{sym} forms a spherical t -design with $t = 2S_E = 2k$, then we have $\nu_k(\mu) = 2/(2k+1)$, so the above equation (cf. Eq. (91)) reduces to

$$\nu(\Omega(\mu, \mathcal{M}, p)) \geq \frac{4\gamma}{nk(2k+1)}. \quad (94)$$

This inequality is saturated if \mathcal{M} corresponds to the trivial edge coloring and p is uniform. In conjunction with Eq. (5), it is straightforward to derive the number of tests required to achieve a given precision.

VI. VERIFICATION OF 1D AKLT STATES

In this section we discuss in more detail the verification of 1D AKLT states, that is, AKLT states defined on the closed chain (cycle) and open chain.

A. Verification of the AKLT state on the closed chain

1. Simplest verification protocols

Let $G(V, E)$ be the closed chain with n vertices. Given a bond verification protocol specified by a probability distribution μ on the unit sphere, then a verification protocol of the AKLT state $|\Psi_G\rangle$ is specified by a weighted matching cover of G . The simplest matching cover, denoted by \mathcal{M}_T , corresponds to the trivial edge coloring and consists of n matchings, each of which consists of only one edge as illustrated in Fig. 4. Accordingly, each test operator is associated with one edge. Denote by T_j the test operator associated with the edge $\{j, j+1\}$ (here $n+1$ is identified with 1 under the periodic boundary condition). Note that test operators T_j for $j = 1, 2, \dots, n$ are related to each other by cyclic permutations, so they should be performed with the same probability to maximize the spectral gap. The resulting verification operator reads

$$\Omega(\mu, \mathcal{M}_T) = \frac{1}{n} \sum_{j=1}^n T_j(\mu). \quad (95)$$

Figure 5 shows the spectral gap of $\Omega(\mu, \mathcal{M}_T)$ with μ constructed from the five platonic solids; in addition, the figure shows the number of tests required to verify the AKLT state within infidelity $\epsilon = 0.01$ and significance level $\delta = 0.01$.

According to Theorem 5, the spectral gap of $\Omega(\mu, \mathcal{M}_T)$ satisfies

$$\nu(\Omega(\mu, \mathcal{M}_T)) \geq \frac{\nu_2(\mu)\gamma(H^\circ(n))}{n}; \quad (96)$$

here $\nu_2(\mu)$ denotes the spectral gap (from the maximum eigenvalue 1) of the bond verification operator, while $\gamma(H^\circ(n))$ denotes the spectral gap of the Hamiltonian (from the minimum eigenvalue corresponding to the ground state). By virtue of Theorem 2 and Eq. (96) we can further deduce that

$$\nu(\Omega(\mu, \mathcal{M}_T)) \geq \frac{c_k \nu_2(\mu)}{n}, \quad n > 2k, \quad (97)$$

where c_k is defined in Eq. (45). So the number of tests required to verify the AKLT state $|\Psi_G\rangle$ within infidelity

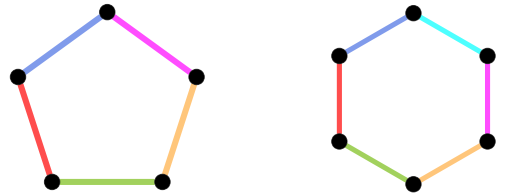


FIG. 4. Trivial edge colorings of closed chains with five and six vertices.

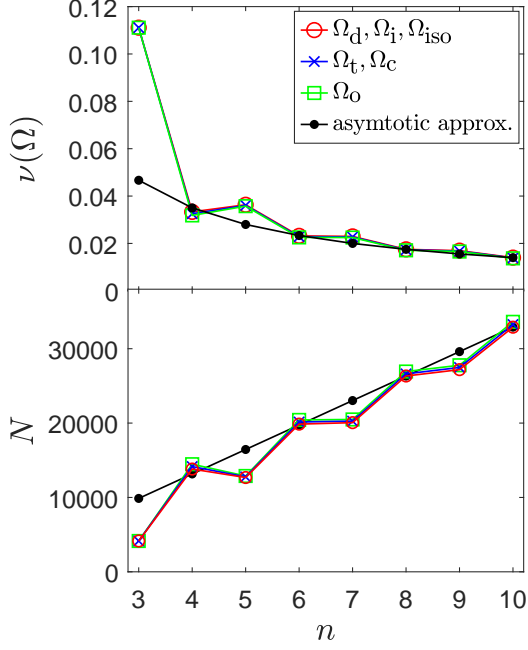


FIG. 5. Spectral gap $\nu(\Omega(\mu, \mathcal{M}_T))$ and number N of tests required to verify the AKLT state on the closed chain of n nodes with precision $\delta = \epsilon = 0.01$. Each protocol is based on the trivial edge coloring, and the underlying bond verification protocol is constructed from a platonic solid or the isotropic distribution on the unit sphere as discussed in Sec. IV C and indicated in the legend. The black dots represent the asymptotic approximation presented in Eq. (101).

ϵ and significance level δ satisfies

$$\begin{aligned} N &\leq \left\lceil \frac{\ln(\delta^{-1})}{\nu(\Omega(\mu, \mathcal{M}_T))\epsilon} \right\rceil \leq \left\lceil \frac{n \ln(\delta^{-1})}{\nu_2(\mu)\gamma(H^\circ(n))\epsilon} \right\rceil \\ &\leq \left\lceil \frac{n \ln(\delta^{-1})}{c_k \nu_2(\mu)\epsilon} \right\rceil, \quad n > 2k, \end{aligned} \quad (98)$$

which is linear in the number of spins.

The inequality in Eq. (96) is saturated when μ forms a spherical 4-design (icosahedron and dodecahedron protocols for example), in which case we have $\nu_2(\mu) = 2/5$ and

$$\nu(\Omega(\mu, \mathcal{M}_T)) = \frac{2\gamma(H^\circ(n))}{5n}, \quad (99)$$

$$N \approx \left\lceil \frac{5n \ln(\delta^{-1})}{2\gamma(H^\circ(n))\epsilon} \right\rceil \leq \left\lceil \frac{5n \ln(\delta^{-1})}{2c_k \epsilon} \right\rceil, \quad (100)$$

where the inequality holds whenever $n > 2k$. Although Eq. (99) is derived under the 4-design assumption, calculation shows that it holds with high precision (with deviation less than 5% for $n \leq 10$) for all protocols based on platonic solids, as illustrated in Fig. 5. When $n = 3$ for example, we have $\gamma(H^\circ(n)) = 5/6$ and $\nu(\Omega(\mu, \mathcal{M}_T)) = 1/9$ for all protocols based on platonic solids. This observation indicates that the general lower bound in Eq. (96) is usually not tight when μ does not

form a 4-design. In other words, protocols based on tetrahedron, octahedron, and cube are more efficient than expected; the reason is still not very clear now.

In the large- n limit, the spectral gap $\gamma(H^\circ(n))$ is approximately equal to 0.350 [6, 78]. If in addition μ forms a spherical 4-design, then we have

$$\nu(\Omega(\mu, \mathcal{M}_T)) \approx \frac{0.140}{n}, \quad N \approx \frac{7.14 n \ln(\delta^{-1})}{\epsilon}. \quad (101)$$

Numerical calculation shows that all protocols based on platonic solids can achieve a similar performance as illustrated in Fig. 5.

2. Optimal matching protocols

More efficient verification protocols can be constructed from better matching covers. For the cycle graph G with n vertices, the chromatic index is given by

$$\chi'(G) = \begin{cases} 2 & \text{if } n \text{ is even,} \\ 3 & \text{if } n \text{ is odd.} \end{cases} \quad (102)$$

When n is even, there exist two maximum matchings, namely,

$$\begin{aligned} M_1 &= \{\{1, 2\}, \{3, 4\}, \dots, \{n-1, n\}\}, \\ M_2 &= \{\{2, 3\}, \{4, 5\}, \dots, \{n, 1\}\}, \end{aligned} \quad (103)$$

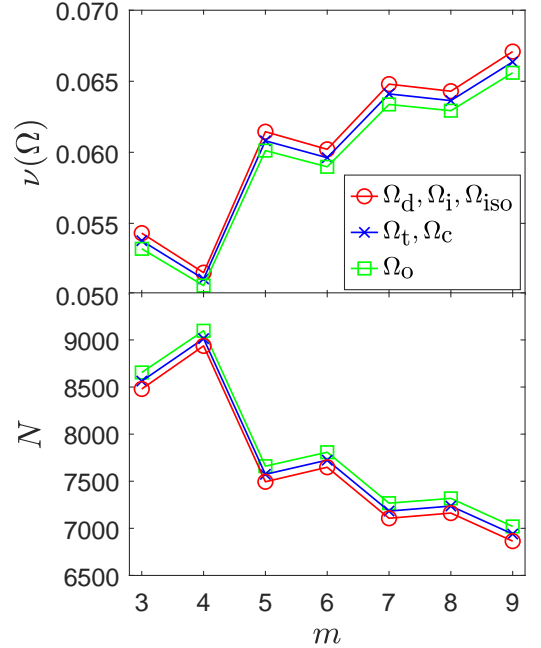


FIG. 6. Verification of the AKLT state on the closed chain of nine nodes based on the matching covers $\mathcal{M}_m = \{M_j\}_{j=1}^m$. Here M_j is the maximum matching defined in Eq. (108), and m is the number of maximum matchings and also the number of distinct tests employed. Infidelity and significance level are chosen to be $\delta = \epsilon = 0.01$ as in Fig. 5; the choice of bond verification protocols is also the same.

TABLE IV. The matching numbers $\nu(G)$ and the numbers of maximal and maximum matchings (shown as triples) for closed chains and open chains of 3 to 10 vertices.

n	3	4	5	6	7	8	9	10
closed chain	(1, 3, 3)	(2, 2, 2)	(2, 5, 5)	(3, 5, 2)	(3, 7, 7)	(4, 10, 2)	(4, 12, 9)	(5, 17, 2)
open chain	(1, 2, 2)	(2, 2, 1)	(2, 3, 3)	(3, 4, 1)	(3, 5, 4)	(4, 7, 1)	(4, 9, 5)	(5, 12, 1)

which form the matching cover $\mathcal{M} = \{M_1, M_2\}$ and also defines an edge coloring of G . Given a probability distribution μ on the unit sphere, then we can construct two test operators $T_{M_1}(\mu), T_{M_2}(\mu)$ according to Eq. (71). By symmetry the two tests should be performed with the same probability to maximize the spectral gap. According to Theorem 4 with $m = g = 2$ and $s = 1/2$, the spectral gap of the resulting verification operator satisfies

$$\begin{aligned} \nu(\Omega(\mu, \mathcal{M})) &\geq \frac{(\sqrt{1+\gamma}-1)\nu_2(\mu)}{2\sqrt{1+\gamma}} \\ &\geq \frac{(\sqrt{1+c_k}-1)\nu_2(\mu)}{2\sqrt{1+c_k}}, \end{aligned} \quad (104)$$

where $\gamma = \gamma(H^\circ(n))$. Here the second inequality follows from Theorem 2 and is applicable for $n > 2k$ and $k > 2$. In the large- n limit, we have $\gamma(H^\circ(n)) \approx 0.350$ [6, 78], so the above equation implies that

$$\nu(\Omega(\mu, \mathcal{M})) \gtrsim 0.0697\nu_2(\mu). \quad (105)$$

If in addition μ forms a 4-design, then $\nu_2(\mu) = 2/5$ and

$$\nu(\Omega(\mu, \mathcal{M})) \gtrsim 0.0279. \quad (106)$$

Accordingly, the number of tests required to verify the AKLT state within infidelity ϵ and significance level δ satisfies

$$N \lesssim \frac{36 \ln(\delta^{-1})}{\epsilon}. \quad (107)$$

Numerical calculation presented in Fig. 7 suggests that the bounds in Eqs. (106) and (107) are tight within a factor of 3.

To construct optimal matching protocols, in principle we need to consider all maximal matchings; see Table IV for the number of maximal matchings when $n = 3, 4, \dots, 10$. Nevertheless, numerical calculation based on Eq. (77) suggests that the above protocol is still optimal even in that case; in other words, other maximal matchings do not help.

When n is odd, each matching of G can contain at most $(n-1)/2$ edges, so at least three matchings are required to cover the edge set. Now, there exist n maximum matchings, namely

$$M_j = \{ \{j, j+1\}, \{j+2, j+3\}, \dots, \{j+n-3, j+n-2\} \}, \quad j = 1, 2, \dots, n, \quad (108)$$

where j and $j+n$ denote the same vertex. All these maximum matchings can be generated from M_1 by cyclic

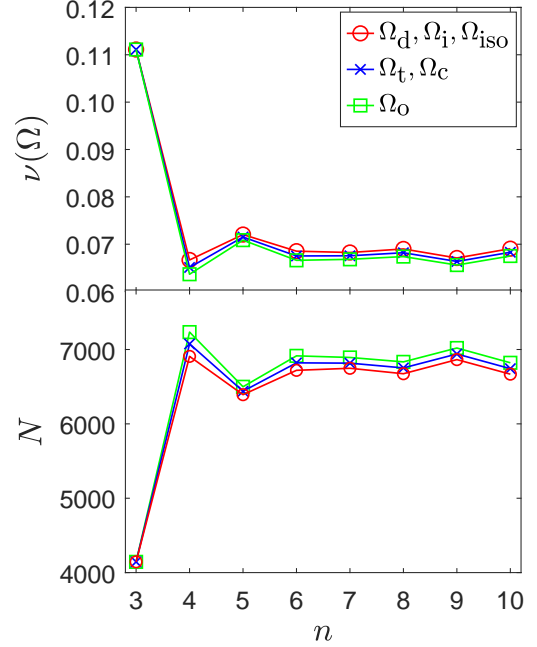


FIG. 7. Verification of the AKLT state on the closed chain based on the matching cover composed of all maximum matchings. Infidelity and significance level are chosen to be $\delta = \epsilon = 0.01$ as in Fig. 5; the choice of bond verification protocols is also the same.

permutations. Let $\mathcal{M}_m = \{M_j\}_{j=1}^m$ for $m = 3, 4, \dots, n$. Then \mathcal{M}_m are matching covers of G and can be employed to construct verification protocols for $|\Psi_G\rangle$. The resulting verification operators are denoted by $\Omega(\mu, \mathcal{M}_m)$. By virtue of Theorem 4 with $g = 2$ and $s = 1/2$ we can deduce that

$$\begin{aligned} \nu(\Omega(\mu, \mathcal{M}_m)) &\geq \frac{(\sqrt{1+\gamma}-1)\nu_2(\mu)}{m(\sqrt{1+\gamma}+1)} \\ &\geq \frac{(\sqrt{1+c_k}-1)\nu_2(\mu)}{m(\sqrt{1+c_k}+1)} \quad m = 3, 4, \dots, n, \end{aligned} \quad (109)$$

where $\gamma = \gamma(H^\circ(n))$. Here the second inequality follows from Theorem 2 and is applicable for $n > 2k$ and $k > 2$. In addition, numerical calculation shows that

$$\nu(\Omega(\mu, \mathcal{M}_{m+2})) \geq \nu(\Omega(\mu, \mathcal{M}_m)), \quad m = 3, 4, \dots, n-2. \quad (110)$$

The performances of these verification protocols are illustrated in Fig. 6.

By symmetry consideration we can deduce that

$$\nu(\Omega(\mu, \mathcal{M}_n)) \geq \nu(\Omega(\mu, \mathcal{M}_m)), \quad m = 3, 4, \dots, n, \quad (111)$$

which implies that

$$\begin{aligned} \nu(\Omega(\mu, \mathcal{M}_n)) &\geq \nu(\Omega(\mu, \mathcal{M}_3)) \geq \frac{(\sqrt{1+\gamma}-1)\nu_2(\mu)}{3(\sqrt{1+\gamma}+1)} \\ &\geq \frac{(\sqrt{1+c_k}-1)\nu_2(\mu)}{3(\sqrt{1+c_k}+1)}, \end{aligned} \quad (112)$$

where the second inequality is applicable when $n > 2k$ and $k > 2$. This bound is slightly worse than the counterpart in Eq. (104), but we believe that Eq. (104) applies for both even n and odd n , and so do Eqs. (105)-(107). Moreover, for a given bond verification protocol μ , the verification operator $\Omega(\mu, \mathcal{M}_n)$ has the largest spectral gap among all verification operators based on maximum matchings. Numerical calculation based on Eq. (77) further suggests that $\Omega(\mu, \mathcal{M}_n)$ is still optimal even if we consider all maximal matchings. The performances of optimal matching protocols are illustrated in Fig. 7.

B. Verification of the AKLT state on the open chain

Next, we turn to the AKLT state on the open chain, which can also be verified following the general approach presented in Sec. III.

1. Simplest verification protocols

Incidentally, when the open chain has two nodes (corresponding to the only connected graph of two vertices), the AKLT Hamiltonian coincides with the projector onto the symmetric subspace of two qubits and has spectral gap equal to 1. The corresponding AKLT state coincides with the singlet. In this case, each matching protocol is just a bond verification protocol. The largest spectral gap is $2/3$, which is achieved when the underlying distribution on the unit sphere forms a spherical 2-design (which is the case for all protocols based on platonic solids). Such

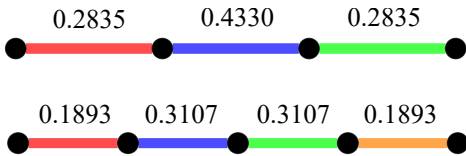


FIG. 8. Trivial edge colorings of open chains with four and five vertices together with the optimal probabilities for performing the tests associated with individual colors. Here the bond verification protocol is built from the dodecahedron.

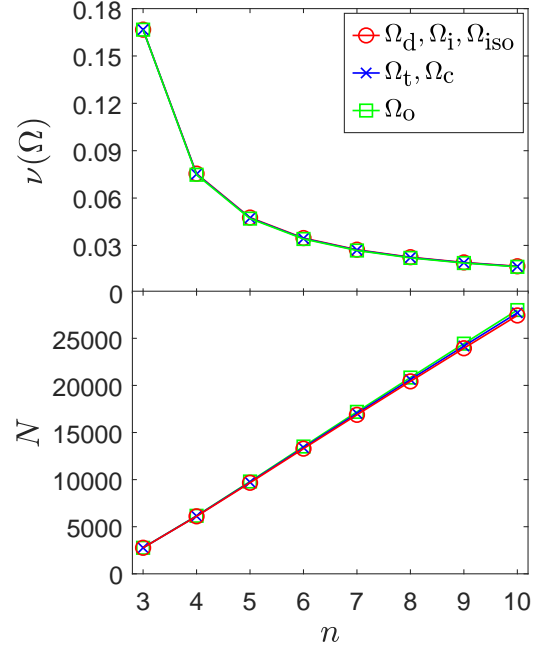


FIG. 9. Verification of the AKLT state on the open chain based on the trivial edge coloring with uniform probabilities. Infidelity and significance level are chosen to be $\delta = \epsilon = 0.01$ as in Fig. 5; the choice of bond verification protocols is also the same.

protocols are also optimal among all protocols based on separable measurements [36, 44].

Many results on the closed chain are still applicable with minor modification for the open chain. First, let us consider verification protocols based on the trivial edge coloring as illustrated in Fig. 8. In this case, Eqs. (95) and (96) are modified as follows,

$$\Omega(\mu, \mathcal{M}_T) = \frac{1}{n-1} \sum_{j=1}^{n-1} T_j(\mu), \quad n \geq 2, \quad (113)$$

$$\nu(\Omega(\mu, \mathcal{M}_T)) \geq \frac{\nu_2(\mu)\gamma(H_{\frac{1}{2}, \frac{1}{2}}(n))}{n-1}, \quad n \geq 3, \quad (114)$$

where μ determines the bond verification protocol. When $n = 3$, $\nu_2(\mu)$ in Eq. (114) can also be replaced by $\nu_{3/2}(\mu)$, which leads to a better lower bound. The performances of several verification protocols based on platonic solids are illustrated in Fig. 9. When μ forms a spherical 4-design (which holds for the icosahedron and dodecahedron protocols), we have $\nu_2(\mu) = 2/5$, so Eq. (114) reduces to

$$\nu(\Omega(\mu, \mathcal{M}_T)) \geq \frac{2\gamma(H_{\frac{1}{2}, \frac{1}{2}}(n))}{5(n-1)}, \quad n \geq 3, \quad (115)$$

which is the counterpart of Eq. (99), but the equality cannot be guaranteed in general.

When $n \geq 4$, in contrast with the closed chain, the optimal probabilities associated with individual colors are not uniform as illustrated in Fig. 8, and the spectral gap

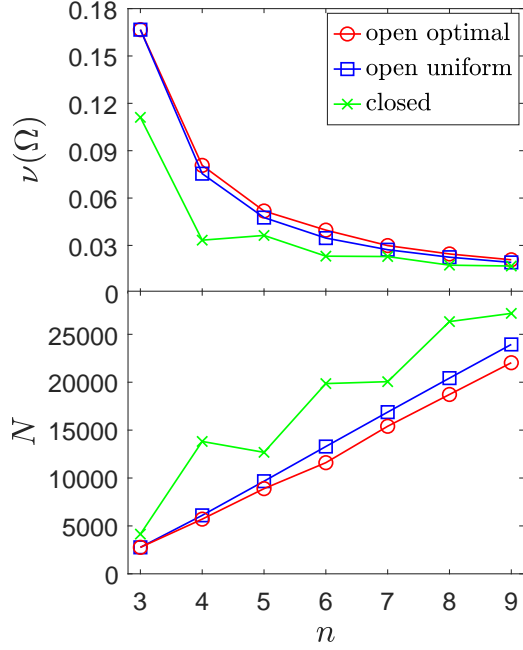


FIG. 10. Verification of the AKLT states on the open chain and closed chain based on the trivial edge coloring with uniform probabilities and optimal probabilities. For the closed chain, the optimal probabilities are uniform. Infidelity and significance level are chosen to be $\delta = \epsilon = 0.01$ as in Fig. 5. The underlying bond verification protocol is built from the dodecahedron.

can be increased by optimizing the probabilities according to Eq. (77), as illustrated in Fig. 10. This figure also shows that it is slightly easier to verify the AKLT state on the open chain than the counterpart on the closed chain.

2. Optimal coloring protocols

To improve the efficiency, we can consider verification protocols based on the optimal coloring. Note that the edges of every open chain can be colored using two colors as illustrated in Fig. 11. When n is odd, the two

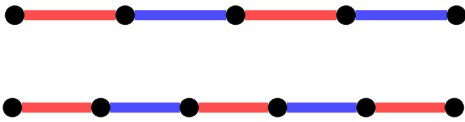


FIG. 11. Optimal edge colorings of open chains with five and six vertices.

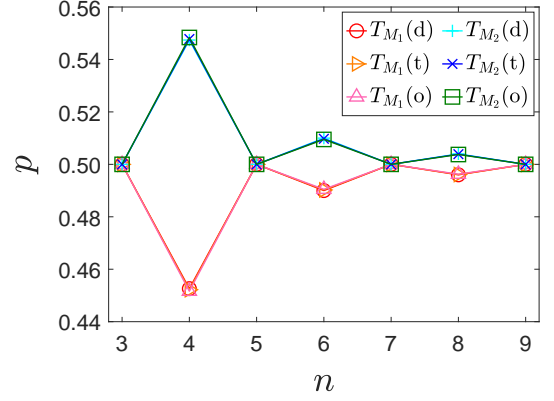


FIG. 12. Optimal probabilities for performing the two tests $T_{M_1}(\mu), T_{M_2}(\mu)$ when the distribution μ is built from the tetrahedron (t), octahedron (o), and dodecahedron (d). Here the two matchings M_1, M_2 are defined in Eqs. (116) and (117).

matchings associated with the optimal coloring read

$$\begin{aligned} M_1 &= \{\{1, 2\}, \{3, 4\}, \dots, \{n-2, n-1\}\}, \\ M_2 &= \{\{2, 3\}, \{4, 5\}, \dots, \{n-1, n\}\}, \end{aligned} \quad (116)$$

which contain the same number of edges. By symmetry the two tests $T_{M_1}(\mu), T_{M_2}(\mu)$ associated with the two matchings should be performed with the same probability to maximize the spectral gap. When n is even, the two matchings read

$$\begin{aligned} M_1 &= \{\{1, 2\}, \{3, 4\}, \dots, \{n-1, n\}\}, \\ M_2 &= \{\{2, 3\}, \{4, 5\}, \dots, \{n-2, n-1\}\}. \end{aligned} \quad (117)$$

In this case the optimal probabilities for performing the two tests $T_{M_1}(\mu), T_{M_2}(\mu)$ are different: they are equal to 0.4900 and 0.5100 when $n = 6$ for example. However, as n increases, the difference gets smaller and smaller as illustrated in Fig. 12, and the improvement brought by probability optimization becomes negligible when $n \geq 8$. Let $\mathcal{M} = \{M_1, M_2\}$; according to Theorem 4 with $m = g = 2$ and $s = 1/2$ ($s = 1/3$ when $n = 3$), in both cases we can deduce that

$$\begin{aligned} \nu(\Omega(\mu, \mathcal{M})) &\geq \frac{(\sqrt{1+\gamma}-1)\nu_2(\mu)}{2\sqrt{1+\gamma}} \\ &\geq \frac{(\sqrt{1+c_k}-1)\nu_2(\mu)}{2\sqrt{1+c_k}}, \end{aligned} \quad (118)$$

where $\gamma = \gamma(H_{\frac{1}{2}, \frac{1}{2}}(n))$. Here the second inequality follows from Theorem 2 and is applicable when $n > 2k$ and $k > 2$. This bound has the same form as the counterpart Eq. (104) for the even closed chain. In addition, Eqs. (105)-(107) are also applicable in the large- n limit as long as $\gamma(H_{\frac{1}{2}, \frac{1}{2}}(n)) \approx \gamma(H^\circ(n))$ (cf. Table I).

Numerical calculation based on Eq. (77) further suggests that the optimal coloring protocol is also optimal among all matching protocols. Figure 13 shows the performance of the optimal matching protocol in comparison

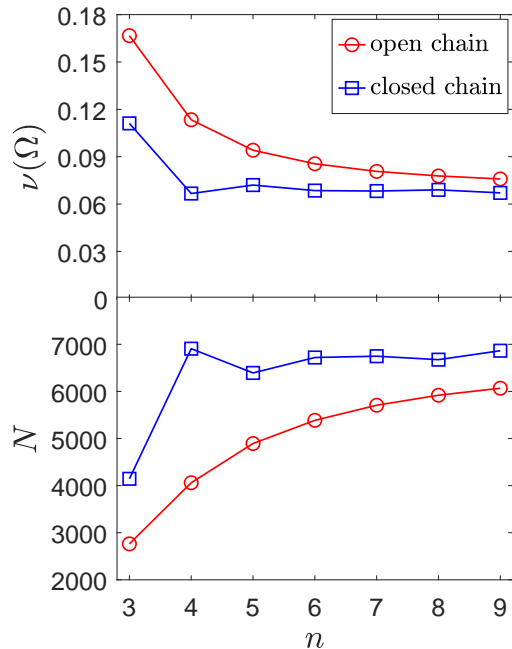


FIG. 13. Verification of the AKLT state on the closed chain and open chain with optimal matching protocols. Infidelity and significance level are chosen to be $\delta = \epsilon = 0.01$ as in Fig. 5. The underlying bond verification protocol is based on the dodecahedron. For the even closed chain and odd open chain, the optimal matching protocol is a coloring protocol with uniform probabilities. For the even open chain, the protocol is a coloring protocol with optimized probabilities. For the odd closed chain, the protocol is based on all maximum matchings with uniform probabilities.

with the counterpart for the closed chain. For a given number of nodes, it is easier to verify the AKLT state on the open chain than the one on the closed chain.

VII. VERIFICATION OF AKLT STATES ON GENERAL GRAPHS

To further illustrate the power of our general approach, here we consider in more detail the verification of AKLT states associated with general connected graphs $G(V, E)$ up to five vertices, that is, $n = |V| \leq 5$. Recall that there are 1 connected graph of two vertices, 2 connected graphs of three vertices, 6 connected graphs of four vertices, and 21 connected graphs of five vertices up to isomorphism. In Table V in Appendix D we have summarized relevant basic information about the 30 graphs and the corresponding AKLT states, including the degree, matching number, chromatic number, chromatic index, the dimension of the underlying Hilbert space, and the spectral gap of the Hamiltonian.

To construct a verification protocol for the AKLT state associated with a given graph, it is essential to choose a suitable bond verification protocol. Here we focus on

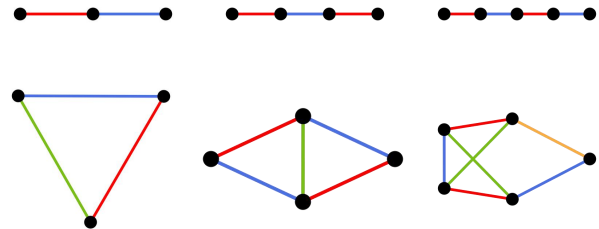


FIG. 14. Connected graphs of three, four, and five vertices for which the verification operators (based on optimized coloring protocols) of the corresponding AKLT states have the largest spectral gaps (up) and smallest spectral gaps (down).

the protocol based on the distribution μ_{32} , which corresponds to the pentakis dodecahedron as described in Sec. IV C. This bond verification protocol can achieve the largest bond spectral gap (as the isotropic protocol) for all edges in graphs up to five vertices, since the corresponding distribution μ_{32} forms a spherical 9-design. Incidentally, for graphs up to four vertices, the alternative bond verification protocol based on the distribution μ_{24} (cf. Sec. IV C) can achieve the same performance.

Given the bond verification protocol, a verification protocol for the AKLT state $|\Psi_G\rangle$ is determined by a matching cover of the underlying graph G . We are particularly interested in coloring protocols, which correspond to matching covers composed of disjoint matchings. The simplest protocol is based on the trivial edge coloring: all edges have different colors. The spectral gap of the resulting verification protocol (with uniform probabilities for all the colors) for each graph up to five vertices is shown in Table V in Appendix D. For comparison, the table also shows the spectral gaps of two verification protocols associated with an optimal edge coloring: one protocol employs the uniform probabilities for all the colors, while the other one employs the optimized probabilities, which can be determined by SDP according to Eq. (77). For each star graph and the 3-cycle, all three protocols coincide with each other, and so do the corresponding spectral gaps. For most other graphs, by contrast, the performance can be improved by considering an optimal edge coloring together with the optimized probabilities. For graphs with a given number of vertices, calculation shows that the spectral gap is maximized at the linear graph as shown in Fig. 14. We have not found a general pattern for the graph that leads to the smallest spectral gap.

Next, we discuss briefly verification protocols based on different bond verification protocols as discussed in Sec. IV C. Figure 15 illustrates the dependence of the spectral gap on the bond verification operator in the case of star graphs with 3 to 10 vertices and complete graphs with 3 to 6 vertices. Here each verification protocol is based on the optimal coloring (which coincides with the trivial coloring for each star graph) with uniform probabilities (which are also optimal). In general, the relative

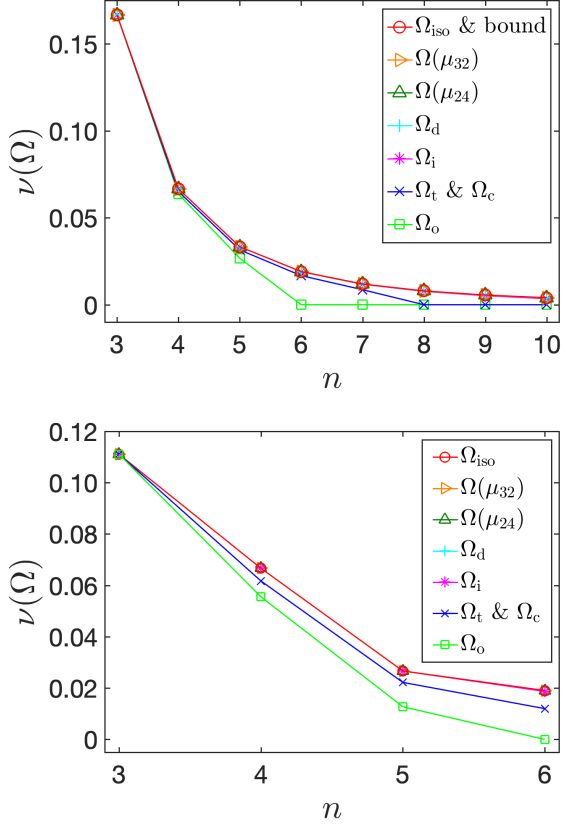


FIG. 15. Spectral gaps of verification operators of AKLT states defined on star graphs with 3 to 10 vertices (upper plot) and complete graphs with 3 to 6 vertices (lower plot). Every verification operator is based on the optimal edge coloring (which coincides with the trivial edge coloring for the star graph) with uniform probabilities (which are also optimal). The bond verification protocols are based on platonic solids, distributions μ_{24}, μ_{32} , and the isotropic distribution defined in Sec. IV C as indicated in the legends. Note that many different bond verification protocols lead to nearly identical spectral gaps. For each star graph, the spectral gap of the verification operator based on the isotropic distribution coincides with the first lower bound in Eq. (90).

deviations in the spectral gaps tend to increase as the number of nodes increases. The spectral gap of the verification operator based on the octahedron (Ω_o) vanishes when $n \geq 6$ for both star graphs and complete graphs. By contrast, the spectral gaps of verification operators based on icosahedron (Ω_i), dodecahedron (Ω_d), distribution μ_{24} ($\Omega(\mu_{24})$), distribution μ_{32} ($\Omega(\mu_{32})$), and isotropic distribution (Ω_{iso}) are close to each other in all the cases under consideration.

VIII. SUMMARY

We proposed a general method for constructing efficient verification protocols for AKLT states defined on

arbitrary graphs based on local spin measurements. Explicit expressions for the AKLT states are not necessary to apply our approach. Given an AKLT state, our verification protocols can be constructed from probability distributions on the unit sphere and matching covers (including edge colorings) of the underlying graph, which have a simple geometric and graphic picture. We also provide rigorous performance guarantee that is required for practical applications. With our approach, most AKLT states of wide interest, including those defined on 1D and 2D lattices, can be verified with constant sample cost, which is independent of the system size and is dramatically more efficient than all approaches known in the literature. Our verification protocols will be useful to various tasks in quantum information processing that employ AKLT states, including measurement-based quantum computation in particular.

ACKNOWLEDGMENTS

H. Zhu is grateful to Zheng Yan and Penghui Yao for stimulating discussions. This work is supported by the National Natural Science Foundation of China (Grants No. 92165109 and No. 11875110) and Shanghai Municipal Science and Technology Major Project (Grant No. 2019SHZDZX01).

Appendix A: Proof of Lemma 1

Proof of Lemma 1. In the special case $\mathbf{r} = \mathbf{s}$, the probability $p_{\mathbf{r},\mathbf{s}}(S_1, m_1; S_2, m_2)$ is independent of the unit vector \mathbf{r} and so can be abbreviated as $p(S_1, m_1; S_2, m_2)$; to simplify the computation, we can assume that $\mathbf{r} = \hat{z}$. Let $S = S_1 + S_2$, $m = m_1 + m_2$, and denote by $|S, m\rangle$ the eigenstate of $S_z = S_{1,z} + S_{2,z}$ with eigenvalue m . Then

$$\begin{aligned} p(S_1, m_1; S_2, m_2) &= |\langle S, m | S_1, m_1; S_2, m_2 \rangle|^2 \\ &= \binom{2S}{2S_1} \binom{S+m}{S_1+m_1} \binom{S-m}{S_1-m_1} \leq 1, \end{aligned} \quad (\text{A1})$$

where the second equality follows from the well known formula for the Clebsch-Gordon coefficients [85]. In addition, the last inequality is saturated iff $m = \pm S$, which means either Eq. (55a) or (55b) holds.

When $\mathbf{r} = -\mathbf{s}$, the inequality $p_{\mathbf{r},\mathbf{s}}(S_1, m_1; S_2, m_2) \leq 1$ is saturated iff either Eq. (55c) or (55d) holds according to the above analysis and following equalities,

$$\begin{aligned} p_{\mathbf{r},\mathbf{s}}(S_1, m_1; S_2, m_2) &= p_{-\mathbf{r},\mathbf{s}}(S_1, -m_1; S_2, m_2) \\ &= p_{\mathbf{r},-\mathbf{s}}(S_1, m_1; S_2, -m_2). \end{aligned} \quad (\text{A2})$$

In general, $|S_2, m_2\rangle_{\mathbf{s}}$ can be expanded as follows,

$$|S_2, m_2\rangle_{\mathbf{s}} = \sum_{k=-S_2}^{S_2} c_k |S_2, k\rangle_{\mathbf{r}}, \quad (\text{A3})$$

where the coefficients c_k satisfy the normalization condition $\sum_{k=-S_2}^{S_2} |c_k|^2 = 1$. Since the projector P_S commutes with $(\mathbf{S}_1 + \mathbf{S}_2) \cdot \mathbf{r}$, it follows that

$$p_{\mathbf{r}, \mathbf{s}}(S_1, m_1; S_2, m_2) = \sum_{k=-S_2}^{S_2} |c_k|^2 p(S_1, m_1; S_2, k) \leq 1, \quad (\text{A4})$$

and the inequality is saturated iff

$$p(S_1, m_1; S_2, k) = 1 \quad \forall c_k \neq 0, \quad (\text{A5})$$

which means $c_k = 0$ whenever $p(S_1, m_1; S_2, k) < 1$.

Recall that $p(S_1, m_1; S_2, k) \leq 1$, and the inequality is saturated iff $m_1 + k = \pm(S_1 + S_2)$. Suppose the inequality in Eq. (A4) is saturated, then $m_1 = \pm S_1$. By symmetry, we also have $m_2 = \pm S_2$. If $m_1 = S_1$, then

$$|c_k| = \begin{cases} 1 & k = S_2, \\ 0 & \text{otherwise,} \end{cases} \quad (\text{A6})$$

which implies that $|S_2, m_2\rangle_{\mathbf{s}} = |S_2, S_2\rangle_{\mathbf{r}}$ up to an overall phase factor, so either Eq. (55a) or (55c) holds in view of Eq. (25). If $m_1 = -S_1$, then either Eq. (55b) or (55d) holds according to a similar reasoning. \square

Appendix B: Proof of Lemma 3

Proof of Lemma 3. To prove Lemma 3, it suffices to prove Eq. (61). According to Eq. (59), we have

$$\nu_{S_j}(\mu) = \lambda_{\min}(O_{S_j}), \quad j = 1, 2, \quad (\text{B1})$$

where

$$O_{S_j} = O_{S_j}(\mu) = 2 \int |S_j\rangle_{\mathbf{r}} \langle S_j| d\mu_{\text{sym}}(\mathbf{r}), \quad j = 1, 2 \quad (\text{B2})$$

according to Eq. (60). Define

$$\begin{aligned} W_j &:= \int \left(\left| \frac{1}{2} \right\rangle_{\mathbf{r}} \left\langle \frac{1}{2} \right| \right)^{\otimes 2S_j} d\mu_{\text{sym}}(\mathbf{r}) \\ &= \int \left(\frac{1 + \mathbf{r} \cdot \boldsymbol{\sigma}}{2} \right)^{\otimes 2S_j} d\mu_{\text{sym}}(\mathbf{r}), \quad j = 1, 2, \end{aligned} \quad (\text{B3})$$

where $\boldsymbol{\sigma} = (\sigma_x, \sigma_y, \sigma_z)$ is the vector composed of the three Pauli operators. Then W_j for each j is a positive semidefinite operator acting on the symmetric subspace of $\mathbb{C}^{\otimes 2S_j}$. Note that this symmetric subspace has dimension $2S_j + 1$, which is the same as the Hilbert space associated with spin value S_j . In addition, W_1 is the partial trace of W_2 after tracing out $2(S_2 - S_1)$ qubits. Moreover, W_j and O_{S_j} have the same nonzero eigenvalues, including multiplicities. Let Π_{2S_j} be the projector onto the symmetric subspace of $\mathbb{C}^{\otimes 2S_j}$; then

$$\nu_{S_j}(\mu) = \lambda_{\min}(O_{S_j}) = \max\{\lambda | W_j \geq \lambda \Pi_{2S_j}\}. \quad (\text{B4})$$

Notably, we have

$$W_2 \geq \nu_{S_2}(\mu) \Pi_{2S_2}. \quad (\text{B5})$$

Taking partial trace over $2(S_2 - S_1)$ qubits we can deduce that

$$W_1 \geq \nu_{S_2}(\mu) \frac{2S_2 + 1}{2S_1 + 1} \Pi_{2S_1}, \quad (\text{B6})$$

which implies Eq. (61) and completes the proof of Lemma 3. \square

Appendix C: Proof of Theorem 3

Proof of Theorem 3. From the definition in Eq. (58) we can deduce that

$$\text{tr}[\Omega_S(\mu)] = 2S - 1. \quad (\text{C1})$$

Suppose statement 1 holds; then

$$\|\Omega_S(\mu)\| = \frac{2S - 1}{2S + 1} = \frac{\text{tr}[\Omega_S(\mu)]}{2S + 1}, \quad (\text{C2})$$

according to Eq. (59), so statement 2 must hold given that $\Omega_S(\mu)$ is a positive operator acting on a Hilbert space of dimension $2S + 1$. The implication $2 \Rightarrow 3$ is obvious.

Next, if $\Omega_S(\mu)$ is proportional to the identity operator, then both statements 1 and 2 hold by Eq. (C1). It follows that statements 1, 2, 3 are equivalent to each other.

To complete the proof, it remains to show the equivalence of statements 2 and 4. If statement 2 holds, then

$$\text{tr}[\Omega_S(\mu)^2] = \frac{(2S - 1)^2}{2S + 1}. \quad (\text{C3})$$

So statement 4 holds according to Lemma 4 below.

Conversely, suppose μ_{sym} forms a spherical t -design with $t = 2S$. By virtue of Lemma 4 below we can deduce

$$\text{tr}[\Omega_S(\mu)^2] = \frac{(2S - 1)^2}{2S + 1} = \frac{1}{2S + 1} \text{tr}[\Omega_S(\mu)]^2, \quad (\text{C4})$$

which implies statement 2 given that $\Omega_S(\mu)$ is a positive operator acting on a Hilbert space of dimension $2S + 1$. This observation completes the proof of Theorem 3. \square

In the rest of this appendix we prove the following lemma, which is employed in the proof of Theorem 3.

Lemma 4. Suppose μ is a probability distribution on the unit sphere. Then the operator $\Omega_S(\mu)$ satisfies

$$\text{tr}[\Omega_S(\mu)^2] \geq \frac{(2S - 1)^2}{2S + 1}; \quad (\text{C5})$$

the inequality is saturated iff the distribution μ_{sym} forms a spherical t -design with $t = 2S$.

Proof of Lemma 4. The inequality in Eq. (C5) follows from Eq. (C1) and the fact that $\Omega_S(\mu)$ is a positive operator acting on a Hilbert space of dimension $2S + 1$. By virtue of Eqs. (58) and (25) in the main text, we can deduce that

$$\begin{aligned}
\text{tr}[\Omega_S(\mu)^2] &= \text{tr} \left\{ \left[1 - 2 \int |S\rangle_{\mathbf{r}} \langle S| d\mu_{\text{sym}}(\mathbf{r}) \right]^2 \right\} \\
&= 2S - 3 + 4 \iint |\mathbf{r}\langle S|S\rangle_{\mathbf{s}}|^2 d\mu_{\text{sym}}(\mathbf{r}) d\mu_{\text{sym}}(\mathbf{s}) \\
&= 2S - 3 + 4 \iint \left(\frac{1 + \mathbf{r} \cdot \mathbf{s}}{2} \right)^{2S} d\mu_{\text{sym}}(\mathbf{r}) d\mu_{\text{sym}}(\mathbf{s}) \\
&= 2S - 3 + 2^{2-2S} \sum_{j=0}^{\lfloor S \rfloor} \binom{2S}{2j} f_{2j}(\mu_{\text{sym}}) \\
&= 2S - 3 + 2^{2-2S} \sum_{j=0}^{\lfloor S \rfloor} \binom{2S}{2j} f_{2j}(\mu), \tag{C6}
\end{aligned}$$

where

$$f_t(\mu) := \iint d\mu(\mathbf{r}) d\mu(\mathbf{s}) (\mathbf{r} \cdot \mathbf{s})^t \tag{C7}$$

denotes the t th frame potential of the distribution μ , assuming that t is a nonnegative integer. By convention we have $f_0(\mu) = 1$ for any distribution μ .

When t is even, the frame potential $f_t(\mu)$ satisfies the following inequality [82, 83],

$$f_t(\mu) = f_t(\mu_{\text{sym}}) \geq \frac{1}{t+1}, \tag{C8}$$

and the inequality is saturated if μ_{sym} forms a spherical t -design. Combining Eqs. (C6) and (C8) we can deduce that

$$\begin{aligned}
\text{tr}[\Omega_S(\mu)^2] &\geq 2S - 3 + 2^{2-2S} \sum_{j=0}^{\lfloor S \rfloor} \binom{2S}{2j} \frac{1}{2j+1} \\
&= 2S - 3 + \frac{2^{2-2S}}{2S+1} \sum_{j=0}^{\lfloor S \rfloor} \binom{2S+1}{2j+1} \\
&= 2S - 3 + \frac{4}{2S+1} = \frac{(2S-1)^2}{2S+1}, \tag{C9}
\end{aligned}$$

which confirms the inequality in Eq. (C5) again.

Suppose the symmetrized probability distribution μ_{sym} forms a spherical t -design with $t = 2S$, then we have

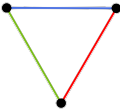
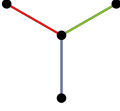
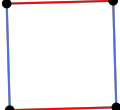
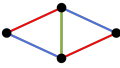
$$f_{2j}(\mu) = f_{2j}(\mu_{\text{sym}}) = \frac{1}{2j+1}, \quad j = 0, 1, \dots, \lfloor S \rfloor. \tag{C10}$$

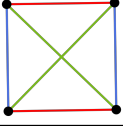
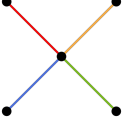
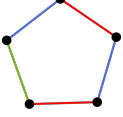
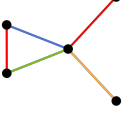
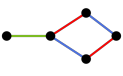
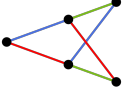
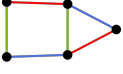
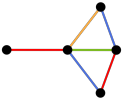
Consequently, the inequality in Eq. (C9) is saturated, which means the inequality in Eq. (C5) is also saturated.

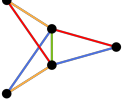
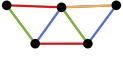
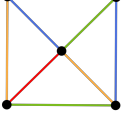
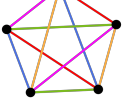
To prove the other direction, suppose the inequality in Eq. (C5) is saturated, so that the inequality in Eq. (C9) is saturated. Then Eq. (C10) must hold, which means μ_{sym} forms a spherical t -design with $t = 2S$ since the distribution μ_{sym} is symmetric under center inversion. \square

Appendix D: Verification of AKLT states on general graphs

TABLE V: Verification of AKLT states on general graphs of two to five vertices. The graphs [86] with optimal edge colorings are shown in the second column. For each graph $\nu(\Omega_{\text{tri}})$ is the spectral gap of the verification operator based on the trivial edge coloring with uniform probabilities; $\nu(\Omega)$ is based on the optimal edge coloring (shown in the second column) with uniform probabilities; $\nu(\tilde{\Omega})$ is based on the optimal edge coloring with optimized probabilities as shown in the last column according to the order: red (R), blue (B), green (G), orange (O), and magenta (M). For graphs No. 1, 2, 3, 4, 7, 9, 10, 11, 18, 27, 30, the optimized probabilities are uniform due to symmetry; for graphs No. 6, 14, 22, 26, the optimized probabilities are uniform by coincidence. All bond verification protocols employed are based on the distribution μ_{32} , which corresponds to the pentakis dodecahedron as described in Sec. IV C. For completeness, the table also shows the vertex number $|V|$, edge number $|E|$, degree $\Delta(G)$, matching number $\nu(G)$, chromatic number $\chi(G)$, chromatic index $\chi'(G)$ of the graph G ; in addition, the table shows the dimension $\dim \mathcal{H}$ of the underlying Hilbert space and the spectral gap $\gamma(H_G)$ of the AKLT Hamiltonian.

No.	graph G	$ V $	$ E $	$\Delta(G)$	$\nu(G)$	$\chi(G)$	$\chi'(G)$	$\dim \mathcal{H}$	$\gamma(H_G)$	$\nu(\Omega_{\text{tri}})$	$\nu(\Omega)$	$\nu(\tilde{\Omega})$	$p(\text{R, B, G, O, M})$
1		2	1	1	1	2	1	4	1	$\frac{2}{3}$	$\frac{2}{3}$	$\frac{2}{3}$	(1)
2		3	2	2	1	2	2	12	$\frac{2}{3}$	$\frac{1}{6}$	$\frac{1}{6}$	$\frac{1}{6}$	$\frac{1}{2} \begin{pmatrix} 1 \\ 1 \end{pmatrix}$
3		3	3	2	1	3	3	27	$\frac{5}{6}$	$\frac{1}{9}$	$\frac{1}{9}$	$\frac{1}{9}$	$\frac{1}{3} \begin{pmatrix} 1 \\ 1 \\ 1 \end{pmatrix}$
4		4	3	3	1	2	3	32	$\frac{1}{2}$	$\frac{1}{15}$	$\frac{1}{15}$	$\frac{1}{15}$	$\frac{1}{3} \begin{pmatrix} 1 \\ 1 \\ 1 \end{pmatrix}$
5		4	3	2	2	2	2	36	0.5168	0.0755	0.1119	0.1134	$\begin{pmatrix} 0.4526 \\ 0.5474 \end{pmatrix}$
6		4	4	3	2	3	3	72	0.5595	$\frac{1}{20}$	$\frac{1}{15}$	$\frac{1}{15}$	$\frac{1}{3} \begin{pmatrix} 1 \\ 1 \\ 1 \end{pmatrix}$
7		4	4	2	2	2	2	81	$\frac{1}{3}$	$\frac{1}{30}$	$\frac{1}{15}$	$\frac{1}{15}$	$\frac{1}{2} \begin{pmatrix} 1 \\ 1 \end{pmatrix}$
8		4	5	3	2	3	3	144	$\frac{1}{2}$	$\frac{1}{30}$	0.0556	0.0618	$\begin{pmatrix} 0.3708 \\ 0.3708 \\ 0.2583 \end{pmatrix}$

No.	graph G	$ V $	$ E $	$\Delta(G)$	$v(G)$	$\chi(G)$	$\chi'(G)$	$\dim \mathcal{H}$	$\gamma(H_G)$	$\nu(\Omega_{\text{tri}})$	$\nu(\Omega)$	$\nu(\tilde{\Omega})$	$p(\text{R, B, G, O, M})$
9		4	6	3	2	4	3	256	$\frac{7}{10}$	$\frac{1}{30}$	$\frac{1}{15}$	$\frac{1}{15}$	$\frac{1}{3} \begin{pmatrix} 1 \\ 1 \\ 1 \end{pmatrix}$
10		5	4	4	1	2	4	80	$\frac{2}{5}$	$\frac{1}{30}$	$\frac{1}{30}$	$\frac{1}{30}$	$\frac{1}{4} \begin{pmatrix} 1 \\ 1 \\ 1 \\ 1 \end{pmatrix}$
11		5	4	2	2	2	2	108	0.4539	0.0476	0.0941	0.0941	$\frac{1}{2} \begin{pmatrix} 1 \\ 1 \end{pmatrix}$
12		5	4	3	2	2	3	96	0.4117	0.0385	0.0511	0.0529	$\begin{pmatrix} 0.3170 \\ 0.4018 \\ 0.2812 \end{pmatrix}$
13		5	5	2	2	3	3	243	0.4540	0.0363	0.0597	0.0603	$\begin{pmatrix} 0.3368 \\ 0.3368 \\ 0.3264 \end{pmatrix}$
14		5	5	4	2	3	4	180	0.4295	$\frac{2}{75}$	$\frac{1}{30}$	$\frac{1}{30}$	$\frac{1}{4} \begin{pmatrix} 1 \\ 1 \\ 1 \\ 1 \end{pmatrix}$
15		5	5	3	2	3	3	192	0.4796	0.0316	0.0527	0.0547	$\begin{pmatrix} 0.2975 \\ 0.2975 \\ 0.4050 \end{pmatrix}$
16		5	5	3	2	2	3	216	0.2871	0.0206	0.0344	0.0369	$\begin{pmatrix} 0.3892 \\ 0.3892 \\ 0.2214 \end{pmatrix}$
17		5	5	3	2	3	3	216	0.4396	0.0308	0.0511	0.0529	$\begin{pmatrix} 0.3122 \\ 0.4018 \\ 0.2860 \end{pmatrix}$
18		5	6	3	2	2	3	432	0.1931	0.0107	0.0214	0.0214	$\frac{1}{3} \begin{pmatrix} 1 \\ 1 \\ 1 \end{pmatrix}$
19		5	6	3	2	3	3	432	0.3106	0.0172	0.0343	0.0347	$\begin{pmatrix} 0.3130 \\ 0.3130 \\ 0.3740 \end{pmatrix}$
20		5	6	4	2	3	4	360	0.42	0.0208	0.0312	0.0319	$\begin{pmatrix} 0.2470 \\ 0.2721 \\ 0.2134 \\ 0.2674 \end{pmatrix}$

No.	graph G	$ V $	$ E $	$\Delta(G)$	$v(G)$	$\chi(G)$	$\chi'(G)$	$\dim \mathcal{H}$	$\gamma(H_G)$	$\nu(\Omega_{\text{tri}})$	$\nu(\Omega)$	$\nu(\tilde{\Omega})$	$p(\text{R, B, G, O, M})$
21		5	6	3	2	3	3	384	0.4036	0.0211	0.0422	0.0441	$\begin{pmatrix} 0.2481 \\ 0.3760 \\ 0.3760 \end{pmatrix}$
22		5	6	4	2	3	4	405	$\frac{7}{15}$	0.0222	$\frac{1}{30}$	$\frac{1}{30}$	$\frac{1}{5} \begin{pmatrix} 1 \\ 1 \\ 1 \\ 1 \\ 1 \end{pmatrix}$
23		5	7	4	2	3	4	675	0.3236	0.0132	0.0231	0.0265	$\begin{pmatrix} 0.2873 \\ 0.2873 \\ 0.1382 \\ 0.2873 \end{pmatrix}$
24		5	7	4	2	3	4	720	0.4263	0.0180	0.0315	0.0318	$\begin{pmatrix} 0.2657 \\ 0.2462 \\ 0.2387 \\ 0.2494 \end{pmatrix}$
25		5	7	3	2	3	4	768	0.2501	0.0110	0.0192	0.0193	$\begin{pmatrix} 0.2625 \\ 0.2375 \\ 0.2625 \\ 0.2375 \end{pmatrix}$
26		5	7	4	2	4	4	640	0.4877	0.0190	$\frac{1}{30}$	$\frac{1}{30}$	$\frac{1}{4} \begin{pmatrix} 1 \\ 1 \\ 1 \\ 1 \end{pmatrix}$
27		5	8	4	2	3	4	1280	0.2836	0.0100	0.0199	0.0199	$\frac{1}{4} \begin{pmatrix} 1 \\ 1 \\ 1 \\ 1 \end{pmatrix}$
28		5	8	4	2	4	4	1200	0.4053	0.0135	0.0269	0.0298	$\begin{pmatrix} 0.2818 \\ 0.2818 \\ 0.1687 \\ 0.2677 \end{pmatrix}$
29		5	9	4	2	4	5	2000	$\frac{2}{5}$	0.0111	0.02	0.0203	$\begin{pmatrix} 0.1850 \\ 0.1965 \\ 0.1850 \\ 0.2372 \\ 0.1965 \end{pmatrix}$
30		5	10	4	2	5	5	3125	$\frac{3}{5}$	0.0133	$\frac{2}{75}$	$\frac{2}{75}$	$\frac{1}{5} \begin{pmatrix} 1 \\ 1 \\ 1 \\ 1 \\ 1 \end{pmatrix}$

- [1] D. T. Stephen, D.-S. Wang, A. Prakash, T.-C. Wei, and R. Raussendorf, Computational power of symmetry-protected topological phases, *Phys. Rev. Lett.* **119**, 010504 (2017).
- [2] T.-C. Wei, Quantum spin models for measurement-based quantum computation, *Adv. Phys.: X* **3**, 1461026 (2018).
- [3] D. T. Stephen, H. P. Nautrup, J. Bermejo-Vega, J. Eisert,

and R. Raussendorf, Subsystem symmetries, quantum cellular automata, and computational phases of quantum matter, *Quantum* **3**, 142 (2019).

- [4] A. K. Daniel, R. N. Alexander, and A. Miyake, Computational universality of symmetry-protected topologically ordered cluster phases on 2D Archimedean lattices, *Quantum* **4**, 228 (2020).

- [5] M. Goihl, N. Walk, J. Eisert, and N. Tarantino, Harnessing symmetry-protected topological order for quantum memories, *Phys. Rev. Research* **2**, 013120 (2020).
- [6] T.-C. Wei, R. Raussendorf, and I. Affleck, Some aspects of Affleck-Kennedy-Lieb-Tasaki models: tensor network, physical properties, spectral gap, deformation, and quantum computation (2022), arXiv:2201.09307.
- [7] I. Affleck, T. Kennedy, E. H. Lieb, and H. Tasaki, Rigorous results on valence-bond ground states in antiferromagnets, *Phys. Rev. Lett.* **59**, 799 (1987).
- [8] I. Affleck, T. Kennedy, E. H. Lieb, and H. Tasaki, Valence bond ground states in isotropic quantum antiferromagnets, *Commun. Math. Phys.* **115**, 477–528 (1988).
- [9] F. D. M. Haldane, Continuum dynamics of the 1-D Heisenberg antiferromagnet: Identification with the O(3) nonlinear sigma model, *Phys. Lett. A* **93**, 464 (1983).
- [10] F. D. M. Haldane, Nonlinear field theory of large-spin Heisenberg antiferromagnets: Semiclassically quantized solitons of the one-dimensional easy-axis Néel state, *Phys. Rev. Lett.* **50**, 1153 (1983).
- [11] A. N. Kirillov and V. E. Korepin, The valence bond solid in quasicrystals (2009), arXiv:0909.2211.
- [12] Y. Xu and V. E. Korepin, Entanglement of the valence-bond-solid state on an arbitrary graph, *J. Phys. A: Math. Theor.* **41**, 505302 (2008).
- [13] V. E. Korepin and Y. Xu, Entanglement in valence-bond-solid states, *I. J. Mod. Phys. B* **24**, 1361 (2010).
- [14] X. Chen, Z.-C. Gu, Z.-X. Liu, and X.-G. Wen, Symmetry-protected topological orders in interacting Bosonic systems, *Science* **338**, 1604 (2012).
- [15] T. Senthil, Symmetry-protected topological phases of quantum matter, *Annu. Rev. Condens. Matter Phys.* **6**, 299 (2015).
- [16] C.-K. Chiu, J. C. Y. Teo, A. P. Schnyder, and S. Ryu, Classification of topological quantum matter with symmetries, *Rev. Mod. Phys.* **88**, 035005 (2016).
- [17] R. Raussendorf and H. J. Briegel, A one-way quantum computer, *Phys. Rev. Lett.* **86**, 5188 (2001).
- [18] R. Kaltenbaek, J. Lavoie, B. Zeng, S. D. Bartlett, and K. J. Resch, Optical one-way quantum computing with a simulated valence-bond solid, *Nat. Phys.* **6**, 850 (2010).
- [19] T.-C. Wei, I. Affleck, and R. Raussendorf, Affleck-Kennedy-Lieb-Tasaki state on a honeycomb lattice is a universal quantum computational resource, *Phys. Rev. Lett.* **106**, 070501 (2011).
- [20] A. Miyake, Quantum computational capability of a 2D valence bond solid phase, *Ann. Phys.* **326**, 1656 (2011).
- [21] T.-C. Wei, I. Affleck, and R. Raussendorf, Two-dimensional Affleck-Kennedy-Lieb-Tasaki state on the honeycomb lattice is a universal resource for quantum computation, *Phys. Rev. A* **86**, 032328 (2012).
- [22] J. Eisert, D. Hangleiter, N. Walk, I. Roth, D. Markham, R. Parekh, U. Chabaud, and E. Kashefi, Quantum certification and benchmarking, *Nat. Rev. Phys.* **2**, 382–390 (2020).
- [23] J. Carrasco, A. Elben, C. Kokail, B. Kraus, and P. Zoller, Theoretical and experimental perspectives of quantum verification, *PRX Quantum* **2**, 010102 (2021).
- [24] M. Kliesch and I. Roth, Theory of quantum system certification, *PRX Quantum* **2**, 010201 (2021).
- [25] X.-D. Yu, J. Shang, and O. Gühne, Statistical methods for quantum state verification and fidelity estimation, *Adv. Quantum Technol.* **2022**, 2100126 (2022).
- [26] J. Morris, V. Saggio, A. Gočanin, and B. Dakić, Quantum verification and estimation with few copies, *Adv. Quantum Technol.* **2022**, 2100118 (2022).
- [27] D. Gross, Y.-K. Liu, S. T. Flammia, S. Becker, and J. Eisert, Quantum state tomography via compressed sensing, *Phys. Rev. Lett.* **105**, 150401 (2010).
- [28] S. T. Flammia and Y.-K. Liu, Direct fidelity estimation from few Pauli measurements, *Phys. Rev. Lett.* **106**, 230501 (2011).
- [29] M. P. da Silva, O. Landon-Cardinal, and D. Poulin, Practical characterization of quantum devices without tomography, *Phys. Rev. Lett.* **107**, 210404 (2011).
- [30] S. Aaronson, Shadow tomography of quantum states, in *Proceedings of the 50th Annual ACM SIGACT Symposium on Theory of Computing, STOC 2018 (ACM, 2018)* p. 325–338.
- [31] H.-Y. Huang, R. Kueng, and J. Preskill, Predicting many properties of a quantum system from very few measurements, *Nat. Phys.* **16**, 1050 (2020).
- [32] M. Hayashi, K. Matsumoto, and Y. Tsuda, A study of LOCC-detection of a maximally entangled state using hypothesis testing, *J. Phys. A: Math. Gen.* **39**, 14427 (2006).
- [33] M. Cramer, M. B. Plenio, S. T. Flammia, R. Somma, D. Gross, S. D. Bartlett, O. Landon-Cardinal, D. Poulin, and Y.-K. Liu, Efficient quantum state tomography, *Nat. Commun.* **1**, 149 (2010).
- [34] L. Aolita, C. Gogolin, M. Kliesch, and J. Eisert, Reliable quantum certification of photonic state preparations, *Nat. Commun.* **6**, 8498 (2015).
- [35] D. Hangleiter, M. Kliesch, M. Schwarz, and J. Eisert, Direct certification of a class of quantum simulations, *Quantum Sci. Technol.* **2**, 015004 (2017).
- [36] S. Pallister, N. Linden, and A. Montanaro, Optimal verification of entangled states with local measurements, *Phys. Rev. Lett.* **120**, 170502 (2018).
- [37] Y. Takeuchi and T. Morimae, Verification of many-qubit states, *Phys. Rev. X* **8**, 021060 (2018).
- [38] H. Zhu and M. Hayashi, Efficient verification of pure quantum states in the adversarial scenario, *Phys. Rev. Lett.* **123**, 260504 (2019).
- [39] H. Zhu and M. Hayashi, General framework for verifying pure quantum states in the adversarial scenario, *Phys. Rev. A* **100**, 062335 (2019).
- [40] Y.-D. Wu, G. Bai, G. Chiribella, and N. Liu, Efficient verification of continuous-variable quantum states and devices without assuming identical and independent operations, *Phys. Rev. Lett.* **126**, 240503 (2021).
- [41] Y.-C. Liu, J. Shang, R. Han, and X. Zhang, Universally optimal verification of entangled states with nondemolition measurements, *Phys. Rev. Lett.* **126**, 090504 (2021).
- [42] A. Gočanin, I. Šupić, and B. Dakić, Sample-efficient device-independent quantum state verification and certification, *PRX Quantum* **3**, 010317 (2022).
- [43] M. Hayashi, Group theoretical study of LOCC-detection of maximally entangled states using hypothesis testing, *New J. Phys.* **11**, 043028 (2009).
- [44] H. Zhu and M. Hayashi, Optimal verification and fidelity estimation of maximally entangled states, *Phys. Rev. A* **99**, 052346 (2019).
- [45] Z. Li, Y.-G. Han, and H. Zhu, Efficient verification of bipartite pure states, *Phys. Rev. A* **100**, 032316 (2019).
- [46] K. Wang and M. Hayashi, Optimal verification of two-qubit pure states, *Phys. Rev. A* **100**, 032315 (2019).
- [47] X.-D. Yu, J. Shang, and O. Gühne, Optimal verification

- of general bipartite pure states, npj Quantum Inf. **5**, 112 (2019).
- [48] M. Hayashi and T. Morimae, Verifiable measurement-only blind quantum computing with stabilizer testing, Phys. Rev. Lett. **115**, 220502 (2015).
- [49] K. Fujii and M. Hayashi, Verifiable fault tolerance in measurement-based quantum computation, Phys. Rev. A **96**, 030301(R) (2017).
- [50] M. Hayashi and M. Hajdušek, Self-guaranteed measurement-based quantum computation, Phys. Rev. A **97**, 052308 (2018).
- [51] D. Markham and A. Krause, A simple protocol for certifying graph states and applications in quantum networks (2018), arXiv:1801.05057.
- [52] H. Zhu and M. Hayashi, Efficient verification of hypergraph states, Phys. Rev. Appl. **12**, 054047 (2019).
- [53] Z. Li, Y.-G. Han, and H. Zhu, Optimal verification of Greenberger-Horne-Zeilinger states, Phys. Rev. Appl. **13**, 054002 (2020).
- [54] M. Hayashi and Y. Takeuchi, Verifying commuting quantum computations via fidelity estimation of weighted graph states, New J. Phys. **21**, 093060 (2019).
- [55] Y.-C. Liu, X.-D. Yu, J. Shang, H. Zhu, and X. Zhang, Efficient verification of Dicke states, Phys. Rev. Appl. **12**, 044020 (2019).
- [56] Z. Li, Y.-G. Han, H.-F. Sun, J. Shang, and H. Zhu, Verification of phased Dicke states, Phys. Rev. A **103**, 022601 (2021).
- [57] W.-H. Zhang, C. Zhang, Z. Chen, X.-X. Peng, X.-Y. Xu, P. Yin, S. Yu, X.-J. Ye, Y.-J. Han, J.-S. Xu, G. Chen, C.-F. Li, and G.-C. Guo, Experimental optimal verification of entangled states using local measurements, Phys. Rev. Lett. **125**, 030506 (2020).
- [58] W.-H. Zhang, X. Liu, P. Yin, X.-X. Peng, G.-C. Li, X.-Y. Xu, S. Yu, Z.-B. Hou, Y.-J. Han, J.-S. Xu, Z.-Q. Zhou, G. Chen, C.-F. Li, and G.-C. Guo, Classical communication enhanced quantum state verification, npj Quantum Inf. **6**, 103 (2020).
- [59] L. Lu, L. Xia, Z. Chen, L. Chen, T. Yu, T. Tao, W. Ma, Y. Pan, X. Cai, Y. Lu, S. Zhu, and X.-S. Ma, Three-dimensional entanglement on a silicon chip, npj Quantum Inf. **6**, 30 (2020).
- [60] X. Jiang, K. Wang, K. Qian, Z. Chen, Z. Chen, L. Lu, L. Xia, F. Song, S. Zhu, and X. Ma, Towards the standardization of quantum state verification using optimal strategies, npj Quantum Inf. **6**, 90 (2020).
- [61] Y.-D. Wu and B. C. Sanders, Efficient verification of bosonic quantum channels via benchmarking, New J. Phys. **21**, 073026 (2019).
- [62] Y.-C. Liu, J. Shang, X.-D. Yu, and X. Zhang, Efficient verification of quantum processes, Phys. Rev. A **101**, 042315 (2020).
- [63] H. Zhu and H. Zhang, Efficient verification of quantum gates with local operations, Phys. Rev. A **101**, 042316 (2020).
- [64] P. Zeng, Y. Zhou, and Z. Liu, Quantum gate verification and its application in property testing, Phys. Rev. Research **2**, 023306 (2020).
- [65] R.-Q. Zhang, Z. Hou, J.-F. Tang, J. Shang, H. Zhu, G.-Y. Xiang, C.-F. Li, and G.-C. Guo, Efficient experimental verification of quantum gates with local operations, Phys. Rev. Lett. **128**, 020502 (2022).
- [66] M. Luo, X. Zhang, and X. Zhou, Proof-of-principle experimental demonstration of quantum gate verification, Phys. Rev. A **105**, 012614 (2022).
- [67] M. Gluza, M. Kliesch, J. Eisert, and L. Aolita, Fidelity witnesses for fermionic quantum simulations, Phys. Rev. Lett. **120**, 190501 (2018).
- [68] E. Cruz, F. Baccari, J. Tura, N. Schuch, and J. I. Cirac, Preparation and verification of tensor network states, Phys. Rev. Research **4**, 023161 (2022).
- [69] H. Zhu, Y. Li, and T. Chen, Efficient Verification of Ground States of Frustration-Free Hamiltonians (2022), unpublished.
- [70] W.-M. Zhang, D. H. Feng, and R. Gilmore, Coherent states: Theory and some applications, Rev. Mod. Phys. **62**, 867 (1990).
- [71] V. I. Voloshin, *Introduction to Graph and Hypergraph Theory* (Nova Science Publishers Inc, New York, 2009).
- [72] V. G. Vizing, On an estimate of the chromatic class of a p-graph (Russian), Diskret. Analiz **3**, 25–30 (1964).
- [73] H. Abdul-Rahman, M. Lemm, A. Lucia, B. Nachtergaele, and A. Young, A class of two-dimensional AKLT models with a gap, in *Analytic Trends in Mathematical Physics*, Contemporary Mathematics, Vol. 741, edited by H. Abdul-Rahman, R. Sims, and A. Young (American Mathematical Society, 2020) pp. 1–21.
- [74] N. Pomata and T.-C. Wei, AKLT models on decorated square lattices are gapped, Phys. Rev. B **100**, 094429 (2019).
- [75] N. Pomata and T.-C. Wei, Demonstrating the Affleck-Kennedy-Lieb-Tasaki Spectral Gap on 2D Degree-3 Lattices, Phys. Rev. Lett. **124**, 177203 (2020).
- [76] M. Lemm, A. W. Sandvik, and L. Wang, Existence of a spectral gap in the Affleck-Kennedy-Lieb-Tasaki model on the hexagonal lattice, Phys. Rev. Lett. **124**, 177204 (2020).
- [77] W. Guo, N. Pomata, and T.-C. Wei, Nonzero spectral gap in several uniformly spin-2 and hybrid spin-1 and spin-2 AKLT models, Phys. Rev. Research **3**, 013255 (2021).
- [78] A. Garcia-Saez, V. Murg, and T.-C. Wei, Spectral gaps of Affleck-Kennedy-Lieb-Tasaki Hamiltonians using tensor network methods, Phys. Rev. B **88**, 245118 (2013).
- [79] S. Knabe, Energy gaps and elementary excitations for certain VBS-quantum antiferromagnets, J. Stat. Phys. **52** (1988).
- [80] D. Gosset and E. Mozgunov, Local gap threshold for frustration-free spin systems, J. Math. Phys. **57**, 091901 (2016).
- [81] P. Delsarte, J. M. Goethals, and J. J. Seidel, Spherical codes and designs, Geom. Dedicata **6**, 363 (1977).
- [82] J. J. Seidel, Definitions for spherical designs, J. Stat. Plan. Inference **95**, 307 (2001).
- [83] E. Bannai and E. Bannai, A survey on spherical designs and algebraic combinatorics on spheres, Eur. J. Combinator. **30**, 1392 (2009).
- [84] D. Hughes and S. Waldron, Spherical half-designs of high order, Involve **13**, 193 (2020).
- [85] A. Bohm, *Quantum Mechanics: Foundations and Applications*, 3rd ed. (Springer, New York, 1993).
- [86] B. McKay, Combinatorial data, Website, <http://users.cecs.anu.edu.au/~bdm/data/graphs.html>.